Theoretical and Computational Fluid Dynamics manuscript No.
(will be inserted by the editor)

Yevgeniy Frenkel · Andrew J. Majda · Boualem Khouider

Simple models for the diurnal cycle and convectively coupled waves

Received: date / Accepted: date

Abstract This paper presents a study of the diurnal cycle of tropical precipitation and its interaction with convectively coupled waves in the context of simple models with crude vertical resolution. One and two baroclinic mode models are tested in both the context of a one-column model and the context of full spatial dependency that permits waves to propagate and interact with the diurnal cycle. It is found that a one baroclinic mode model is capable of reproducing a realistic diurnal cycle of tropical precipitation both over land and over the ocean provided an adequate switch function is used to mimic the congestus preconditioning mechanism that operates in the multicloud model of Khouider and Majda. However, a full two baroclinic mode multicloud model is needed to capture the interaction of convectively coupled tropical waves with the diurnal cycle. In a more conventional mass-flux parameterization framework, both one and two baroclinic mode models fail to capture the diurnal cycle of tropical precipitation.

Keywords Diurnal cycle · tropical atmospheric dynamics · convectively coupled waves · Multicloud models · Periodic solutions

PACS First · Second · More

Yevgeniy Frenkel
Department of Mathematics and Center for Atmosphere-Ocean Science, Courant Institute
New York University
251 Mercer Street
New York, NY 10012 USA
Tel.: 212-998-3234
Fax: 212-995-4121
E-mail: frenkel@cims.nyu.edu

Andrew J. Majda
Department of Mathematics and Center for Atmosphere-Ocean Science, Courant Institute
New York University
251 Mercer Street
New York, NY 10012 USA
Tel.: 212-998-3234
Fax: 212-995-3323
E-mail: jonjon@cims.nyu.edu

Boualem Khouider
Department of Mathematics and Statistics
University of Victoria
PO BOX 3045 STN CSC
Victoria, BC
Canada V8W 3P4
Tel. 250-721-7439
Fax. 250-721-8962
E-mail: khouider@math.uvic.ca

1 Introduction

The seasonal and diurnal cycles of solar radiation have a major impact on the local and regional variability of Earth's weather and climate. The diurnal cycle effects atmospheric circulation across a broad range of scales, from mesoscale convective systems [63] to intraseasonal oscillations [56]. It is believed that the diurnal cycle plays an important role in the (re)initialization of the Madden–Julian oscillation (MJO) [20,51].

Early investigations of the diurnal variability of tropical precipitation over land and oceans date back, at least, as far as the early 20's [47] but it has not been a major research focus until recently, likely due to the advent of satellite measurements and computers [33,59,41,48,1,2,17,49,16,53]. Kikuchi and Wang in 2008 [31], through innovative use of empirical orthogonal functions (EOF's), elucidated and confirmed the persistence of three main regimes in the diurnal variation of tropical precipitation. An oceanic regime, characterized by an early morning (6:00 am to 9:00 am local solar time: LST) precipitation peak of relatively weak amplitude is found over the deep waters of the three tropical oceans within the inter-tropical convergence zone (ITCZ), a continental regime with a late afternoon precipitation peak (3:00 pm to 6:00 pm LST) of large amplitude is found over central America and Africa, and a coastal regime is seen along the land-sea boundaries of the maritime continent of Indonesia and Sumatra, South India, West Africa, and Northeast of Brazil. The coastal regime is characterized by a large amplitude precipitation peak that propagates in both directions, perpendicular to the shoreline.

Except from some vague speculations, based merely on physical intuition motivated by a few observations and very rare numerical simulations, the physical mechanisms that govern the three regimes of the diurnal variability of tropical precipitation remain an open problem. While the land regime is associated to a direct thermodynamic response of the surface layer to solar radiation [31] and the land-side coastal regime is thought to be due to landward propagation of mesoscale convective systems and tropical squall lines in the direction of the sea-breeze [32,6,13,31], theories for both the oceanic and the sea-side coastal regimes remain very illusive [64,31]. The proposed mechanisms, for the later regimes, range, respectively, from shortwave to long-wave radiation and from the concavity of the shoreline to the propagation of gravity waves.

Current global and regional numerical models of weather and climate have difficulty in reproducing the diurnal variability of tropical precipitation [46,63,7,55] presumably, due to the misrepresentation of moist-tropical convection by the underlying cumulus parameterizations. Some cloud resolving models (CRMs) show moderate success in capturing the diurnal variability [34], yet this approach is computationally too expensive. Furthermore, the complexity of these models conceals the quintessential mechanisms of the diurnal cycle.

Recently, Frenkel, Khouider and Majda proposed, in a series of two papers [9,10], to use the multicloud model of Khouider and Majda [27,29,22,11] to study the diurnal variability of tropical precipitation. The multicloud convective parameterization is based on three cloud types (congestus, deep, and stratiform). The convective closure of the model takes into account the energy available for congestus and deep convection and uses a non-linear moisture switch that allows natural transitions between congestus and deep convection. The multicloud model is very successful in capturing most of the Wheeler–Kiladis–Takayabu spectrum of convectively coupled waves [54,61] in terms of linear wave theory [27,28] and nonlinear organization of large-scale envelopes mimicking across-scale interactions of the Madden-Julian oscillation (MJO) and convectively coupled waves [27,29], in the idealized context of a simple two baroclinic mode model. Furthermore, the multicloud parameterization has been used in the next generation of the National Center for Atmospheric Research GCM (HOMME) and revealed to be very successful in simulating the MJO and convectively coupled equatorial waves, at a coarse resolution of 170 km, in the idealized case of a uniform SST (aquaplanet) setting [30]. Yet, these parameterizations are simple enough to be able to track down and understand the physical mechanisms at work in the model.

Following the idea of looking for stable one-day periodic solutions when the model is forced by a surface (latent and sensible) heating that mimics the diurnal cycle of solar heating, it is established in [9] that the multicloud model is capable of reproducing the most quintessential features of the diurnal cycle over the ocean, namely, the morning precipitation peak. Moreover, a newer variant of the multicloud model, which is coupled to a full dynamical boundary layer [58] does equally well in

representing the diurnal cycle over the ocean and over land. In the land regime, the model assumes a strong inversion profile, a large Bowen ratio of 0.4 and active mixing of sensible heat due to cumulus entrainment and downdraft fluxes at the top of the well-mixed atmospheric boundary layer (ABL). The resulting diurnal solution is characterized by a pronounced afternoon peak in the precipitation consistent with observations of tropical precipitation over continental regions [10]. In this paper, we are interested in the fundamental question of whether a two vertical mode model with all three cloud types is necessary to (1) reproduce the diurnal cycle of precipitation over the ocean and over land as in [9] and [10] respectively, and (2) capture the interaction of the diurnal cycle with convectively coupled gravity waves. It is found here that one baroclinic mode models, supporting only one cloud type, deep convection, are sufficient for capturing the diurnal cycle over land and ocean provided a moisture switch function is used as a surrogate for the congestus preconditioning. However, unlike full two baroclinic mode model multicloud models, the reduced models fail to adequately represent convectively coupled waves and their eventual interaction with the diurnal cycle.

Moncrieff and Liu [43] already pointed out the importance of the interaction of the dipole heating, i.e, the second baroclinic mode, with a background vertical shear for the large-scale organization and propagation of the diurnal cycle of convection, both over land and over the ocean. While this is beyond the scope of the present study it certainly offers an interesting application which can be addressed in a similar fashion.

The rest of the paper is organized as follows. In Section 2, we briefly review the two multicloud models, with and without boundary layer dynamics, named hereafter WK and KM models, respectively. The two and one vertical baroclinic mode versions of the model are used in this paper and contrasted against more conventional parameterizations as exemplified by Majda and Shefter [37,36], which are also reviewed in Section 2. All models are forced from the surface by the diurnal cycle of solar heating. In this section, we consider solutions for the diurnally varying surface fluxes while the effects of waves and other spatial variations are ignored. The mathematical methodology used here to look for one-day periodic stable solutions, which combines numerical methods of ordinary differential equations (ODEs) and the Floquet theory for nonlinear periodic solutions can be found in [9,10]. In section 3, we present the linear stability for convectively coupled waves for the ocean case in various parameter regimes mimicking changes due to the diurnal forcing using both the one and the two vertical mode models. The linear stability analyses is followed by and a discussion of the nonlinear interaction of diurnal cycle solutions and convectively coupled waves in full two baroclinic mode multicloud models and failure the reduced models to capture such interactions. Finally, a concluding summary and an overall discussion are given in Section 4.

2 Minimal models for the diurnal cycle

This section contains a study of the diurnal cycle in the framework of the multicloud convective parameterizations. In particular, simplified Khouider Majda [29] (hereafter KM) and Waite Khouider [58] (hereafter WK) multicloud models are used in the study. The interested reader is referred to [9, 10] for a study of the diurnal cycle in the full KM and WK models.

The essential features of the KM and WK multicloud models are presented in a unified framework. Following the overview, the KM and WK models are simplified by elimination of the second baroclinic mode of vertical structure and removal of the spatial dependency. This results in one baroclinic mode column models which nonetheless capture the essential features of the diurnal cycle over the ocean and land. As in [9] and [10], we look for stable periodic solutions of the resulting ODE systems forced by the surface sensible and latent heat fluxes associated with the solar radiation. In particular, the Majda and Shefter [37,36] models, also reviewed in this section, serve as paradigm analogs of a conventional GCM mass flux parameterization. The complete details of the column model setup can be found in [9] and [10] along with the description of the algorithm used to solve the resulting ODE boundary value problem. All equations for the multicloud model are given in non-dimensional form where the speed of the first baroclinic Kelvin waves, $c_r \approx 50$ ms^{-1}, is the velocity scale, the equatorial Rossby radius of deformation, $L_e \approx 1500$ km, is the length scale, $T = L_e/c_r \approx 8.33$ hours is the time scale, and $\bar{\alpha} = H_T N^2 \theta_0/\pi g \approx 15$ K is the temperature unit scale.

2.1 Free tropospheric dynamical core and vertical structure of the multicloud models

The multicloud parameterization framework assumes three heating profiles associated with the main cloud types that characterize organized tropical convective systems [20]: cumulus congestus clouds that heat the lower troposphere and cool the upper troposphere, through radiation and detrainment, deep convective towers that heat the whole tropospheric depth, and the associated lagging-stratiform anvils that heat the upper troposphere and cool the lower troposphere, due to evaporation of stratiform rain. Accordingly, Khouider and Majda [27,29] used the momentum and potential temperature equations for the first and second baroclinic modes of vertical structure, that are directly forced by deep convection and both congestus and stratiform clouds, respectively, as a minimal dynamical core that captures the main (linear response) effects of these three cloud types. The dynamical core of the multicloud convective parameterizations used in this paper consists of two coupled and forced shallow water systems. Without the meridional dependency, the equations are given by

$$\partial_t u_j - \partial_x \theta_j = d_j - \frac{1}{\tau_R} u_j, \quad j = 1, 2 \tag{1}$$

$$\partial_t \theta_1 - \partial_x u_1 = \frac{\pi}{2\sqrt{2}} P + S_1 + \frac{\pi}{2\sqrt{2}} E_{\alpha,\beta}, \tag{2}$$

$$\partial_t \theta_2 - \frac{1}{4} \partial_x u_1 = H_c - H_s + S_2. \tag{3}$$

Here H_d, H_s and H_c are the heating rate for deep, stratiform and cumulus congestus clouds. These heating rates are combined into bulk precipitation $P = (2\sqrt{2}/\pi)(H_d + \xi_s H_s + \xi_c H_c)$. The terms $d_j, j = 1, 2$ and $S_j, j = 1, 2$ represent the boundary layer drag and radiative cooling rates associated with the first and second baroclinic modes. It is important to note that in this presentation, we have omitted the discussion of the boundary layer momentum and barotropic mode equations. Therefore, the difference between dynamical cores of KM and WK models reduces to two terms. The sensible heat entrainment flux $E_{\alpha\beta}$, which is unique to the WK model, is discussed in detail in the following subsection. The formulation of the boundary turbulent layer drag takes the form $d_j = -C_d u_0 u_j$ in KM model, where C_d and u_0 are the momentum drag coefficient and strength of turbulent fluctuations. In WK model, the boundary layer drag is parameterized by $d_j = -2\delta_b u_j/\mathrm{T}$. Here, T days is the momentum entrainment time scale and δ_b is the ratio of the height of the boundary layer h_b to the height of the free troposphere H_T.

Formally, the equations in (1) – (3) are obtained by a Galerkin projection of the hydrostatic primitive equations with constant buoyancy frequency and rigid lid boundary conditions onto the first two baroclinic modes of vertical structure. The details of the derivation are found in [27,58]. In (1), $u_j|j = 1, 2$ represent the first and second baroclinic velocities assuming $G(z) = \sqrt{2}\cos(\pi z/H_T)$ and $G(2z) = \sqrt{2}\cos(2\pi z/H_T)$ vertical profiles, respectively, while $\theta_j, j = 1, 2$ are the corresponding potential temperature components with the vertical profiles $-G'(z) = \sqrt{2}\sin(\pi z/H_T)$ and $-2G'(2z) = 2\sqrt{2}\sin(2\pi z/H_T)$ respectively. Therefore, the total velocity field, V, and potential temperature, Θ, are approximated by

$$V \approx \bar{U} + G(z)v_1 + G(2z)v_2 \tag{4}$$

$$\Theta \approx z + G'(z)\theta_1 + 2G'(2z)\theta_2. \tag{5}$$

Fig. 1 shows the schematics of the vertical structure. Note that the vertical velocity is recovered via the continuity equation and accordingly it has a combination of a $\sin(z)$ and a $\sin(2z)$ profiles. Multicloud models additionally carry an equation for the vertically integrated tropospheric moisture content, q, and equations for boundary layer variables: moisture q_b and potential temperature θ_b or alternatively boundary layer equivalent potential temperature $\theta_{eb} = q_b + \theta_b$. To facilitate the discussion of interaction between boundary layer and free troposphere, we must first define the bulk vertical jumps. Following WK notation, these jumps are given by

$$\triangle_s \phi \equiv \phi_s - \phi_b, \qquad \triangle_t \phi \equiv \phi_b - \phi_t, \qquad \triangle_m \phi \equiv \phi_b - \phi_m. \tag{6}$$

Here, ϕ is θ_e, θ or q and s, b, t and m indicate values at the surface, in the ABL, top of the ABL, and the middle troposphere, as shown in Fig. 1. The surface values are prescribed. The potential temperature

at the top of the ABL is obtained by taking a limit $z \to 0^+$ of (5) and therefore is set to zero. The moisture at the top of the ABL is assumed to be proportional to the vertically integrated tropospheric moisture, with proportionality parameter $\kappa = 2$. To model the diurnal cycle over land, the radiative convective equilibrium values of jumps in potential temperature ($\triangle\theta_t$) and moisture ($\triangle q_t$) are set to resemble the potential temperature inversion and moisture drop at the top of ABL, as shown in Fig. 1.

Following [27], the middle tropospheric potential temperature is set to

$$\theta_m = \frac{2\sqrt{2}}{\pi}(\theta_1 + \alpha_2\theta_2). \tag{7}$$

where the term $(2\sqrt{2})/\pi\theta_1$ is derived from averaging of the total potential temperature field Θ over the depth of the free troposphere. Small value for α_2 adds a nonzero contribution from second baroclinic heating mode to θ_m although its vertical average is zero. The middle tropospheric equivalent potential temperature anomaly is defined by adding the averaged free tropospheric moisture to middle tropospheric potential temperature equation and is given by

$$\theta_{em} = q + \theta_m = q + \frac{2\sqrt{2}}{\pi}(\theta_1 + \alpha_2\theta_2). \tag{8}$$

The setup of the average free tropospheric moisture and boundary layer variables is discussed next.

2.2 Boundary layer dynamics and the averaged free tropospheric moisture equation

In the case of the WK model, the system of equations in (1) – (3) is augmented by equations for the boundary layer moisture and the equivalent potential temperature:

$$\partial_t q_b = -\frac{E}{h_b}\triangle_t q - \frac{D_c}{h_b}\triangle_m q + \frac{1}{\tau_e}\triangle_s q, \tag{9}$$

$$\partial_t \theta_b = -\frac{E}{h_b}\triangle_t \theta - \frac{D_c}{h_b}\triangle_m \theta + \frac{1}{\tau_e}\triangle_s \theta - Q_{Rb}. \tag{10}$$

Aside of the constant radiative cooling, the forcing in equations (9) and (10) is due to vertical turbulent fluxes at the top and bottom of the ABL. The turbulent fluxes lead to the entrainment of free tropospheric scalars into the boundary layer. The entrainment velocity is given by $E = M_u - D_c$ where M_u is the upward scalar flux velocity, assumed to be proportional to the mass flux velocity from convective downdraft, D_c. Here the term downdraft refers to the subsiding air resulting from evaporative cooling of stratiform rain in the middle of the troposphere, which therefore results in the moistening of the middle troposphere (increasing q) and drying, and cooling the boundary layer by bringing dry and cold air from aloft. The mass flux velocity for convective downdraft is given by

$$D_c = m_0[1 + \frac{\mu}{\bar{Q}}(H_s - H_c)], \tag{11}$$

where the downdraft mass flux scale, m_0, and the background heating, $\bar{Q}$, are obtained from the radiative convective equilibrium (RCE) solution. A detailed discussion of RCE solutions of KM and WK models can be found in [58,29]. The last two terms of the equation reflect the dynamic balance between the stratiform downdraft and cumulus congestus updraft.

The troposphere moisture equation, q, is derived from the bulk water vapor budget equation by imposing a moisture stratification-like background vertical profile [58,29] and takes the form

$$\frac{\partial q}{\partial t} + \partial_x[(u_1 + \delta u_2)q + (u_1 + \tilde{\lambda}u_2)\tilde{Q}] = -P + D/H_T - E_{1-\alpha,1-\beta}, \tag{12}$$

where

$$D = E\triangle_t q + D_c\triangle_m q + E\triangle_t\theta + D_c\triangle_m\theta = E\triangle_t\theta_e + D_c\triangle_m\theta_e. \tag{13}$$

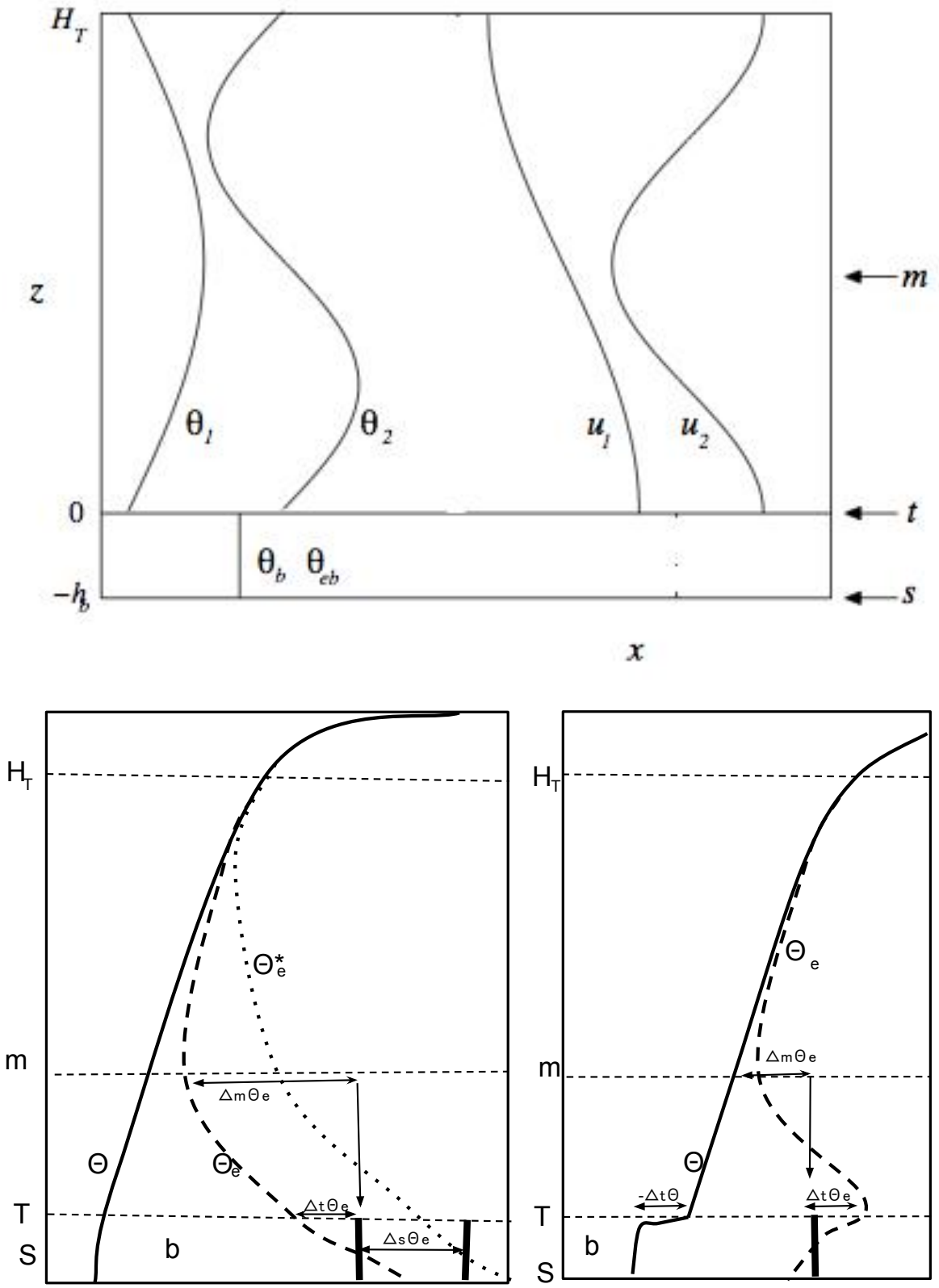

Fig. 1 Schematic of the vertical structure of the multicloud models (top). Schematic drawing of background potential and equivalent potential temperature profiles with RCE fluxes used for the ocean (bottom left) and land (bottom right). Here s, t and m indicate vertical locations where values at the surface, top of the ABL, and the middle troposphere are taken.

The last two terms in (13) represent entrainment and downdrafts, respectively. They account for free-tropospheric moistening due to detrainment of shallow cumulus clouds and evaporation of stratiform rain. The discussion of the moisture convergence (the second term on the right-hand side of (12)) is deferred to Sections 3 and 4. However, it is important to note that in the full WK model, it accounts for large scale downdraft which interacts with the boundary layer dynamics. Nevertheless, as will be shown below, the omission of this mechanism does not significantly influence the timing of the diurnal cycle.

An important element of the WK model, which was first introduced in [9], is the distribution of the entrainment and downdraft fluxes between the free tropospheric moisture and the potential temperature equations. The feature allows penetration of sensible heat fluctuations through the top of the boundary layer interface. In the original WK model, entrainment and downdraft fluxes entering both the ABL moisture and θ_b equations are balanced by similar fluxes in the free-tropospheric moisture equation alone.

The sensible heat entrainment term, $E_{\alpha\beta}$ in (2) and (12), is given by

$$E_{\alpha\beta} = \alpha E \triangle_t \theta + \beta D_c \triangle_m \theta. \tag{14}$$

When α and β are both set to zero no exchange of sensible heat at the top of the AB is possible. The use of larger values $\alpha = \beta = 1/3$ (compared to the zero values used in [58]) can be justified by extra-mixing of sensible heat by gravity waves. These effects are of paramount importance to the correct reproduction of the diurnal cycle over land.

When the radiative cooling rates, S_1, S_2, and the surface fluxes, are set to zero, the equations (1) through (11) automatically have conservation of an approximation to vertically integrated moist static energy. Notice that, the precipitation rate and sensible heat redistribution flux in (2) balances the vertical average of the total convective heating rate and $E_{\alpha\beta}$ in (12). The moistening of the free troposphere by convective downdrafts and entrainment of shallow congestus clouds in (12) is in turn balanced by the drying of boundary layer by the convective downdrafts and detrainment of the ALB air in (9) and (10). This leads to the conservation of the vertical average of the equivalent potential temperature $\langle \theta_e \rangle = \langle Q_z \rangle + q + \langle \Theta \rangle + (h_b/H_T)\theta_{eb}$, here $\langle f \rangle = (1/H_T)\int_0^{H_T} f(z)dz$.

The equations for the boundary layer potential temperature and moisture can be combined into a single equation for the boundary layer equivalent potential temperature,

$$\partial_t \theta_{eb} = -\frac{D_c}{h_b}\triangle_m \theta_e + \frac{1}{\tau_e}\triangle_s \theta_e - Q_{Rb}. \tag{15}$$

The term $(1/\tau_e)\triangle_s \theta_e$ represents the combined effect of the surface sensible and latent heat fluxes. This formulation is particularly useful in modeling convection over the ocean, where the latent heat is the primary response of surface to solar heating. In this case, the evaporation, E_v, is modeled by

$$\frac{1}{\tau_e}\triangle_s \theta_e \equiv \frac{1}{\tau_e}(\theta^*_{eb} - \theta_{eb}) \equiv E_v, \tag{16}$$

where θ^*_{eb} is the saturation equivalent potential temperature. At RCE $\theta^*_{eb} - \theta_{eb}$ is set to 10 K in accordance with the Jordan sounding [21] (also see Fig.1).

The equations above describe the WK model. To recover the KM model, we turn off the shallow cumulus detrainment and sensible heat mixing of the WK model. This amounts to setting $E_{\alpha\beta} = 0$ in (2) and (12) and letting $D = D_c \triangle_m \theta_e$ in (12) and (15) $Q_{Rb} = 0$ in (15).

2.3 Diurnal forcing

A useful quantity in the study of the diurnal cycle is the ratio of fluxes of sensible heat and latent heat (produced by solar heating) known as the Bowen ratio and denoted here as $\bar{\beta}$. Over the ocean, the Bowen ratio is typically less than 0.1 [18,50]. This fact was by exploited by Khouider and Majda in the derivation of the multicloud model[27,29] as reflected in (16).

The relationship between sea surface temperature (SST) and boundary layer saturation equivalent potential temperature perturbation $\hat{\theta}^{*'}_{eb}$ is inferred from the Clausius-Clapeyron equation. Here we use

$\hat{\theta}^*_{eb,\max} = 10^\circ$ C as a value for the ocean based diurnal variation of 3° of sea surface skin temperature (on top of a 25° mean). To accommodate the asymmetry between the day time solar heating and night time radiative cooling, we assume diurnal variation of SST in the form of a half-sine profile so that

$$\theta^{*'}_{eb} = \theta^*_{eb,\max} \begin{cases} \frac{\pi}{\pi-1}[\sin(x+ct) - \frac{1}{\pi}], \text{ if } x + ct \mod (2\pi) < \pi \\ \frac{1}{1-\pi}, \qquad\qquad\qquad \text{if } x + ct \mod (2\pi) > \pi. \end{cases} \tag{17}$$

Here $c = 463$ m s^{-1} donates the average speed with which the peak of solar energy circles the globe.

As in [9], this perturbation is added to the RCE background $\theta^*_{eb} - \theta_{eb} = 10$K. In the case of the WK model, the latent heat flux $\triangle q_b$ is set equal to E_v and the sensible heat flux is set to zero.

While diurnal variability over the ocean is driven by latent heat, over land it is due to both latent and sensible heating. This allows us to take full advantage of the WK model, where effects of the diurnal cycle of solar heating on the ABL are separated into the perturbation to the constant surface values of moisture $\bar{q}_s$ and temperature $\bar{\theta}_s$ so that

$$q_s(x,t) = \bar{q}_s + \hat{q}_s(x,t), \qquad \theta_s(x,t) = \bar{\theta}_s + \hat{\theta}_s(x,t), \tag{18}$$

where t is time and x is space. Here, $\hat{\theta}_s(x,t)$ and $\hat{q}_s(x,t)$ have the same profile as $\theta^{*'}_{eb}$.

In the land regime, we are mostly concerned with the case of equatorial forest where the large transpiration and soil moisture allows for Bowen ratios in the range of $\bar{\beta} = 0.2$ to $\bar{\beta} = 0.4$ [5]. As in [10], the amplitude of the diurnal variation in surface temperature is inferred directly from observations [63] while a Bowen ratio that is appropriate for the Amazon forest [5] is used to approximate the magnitude of the corresponding moisture surface flux perturbations. Accordingly, the perturbations of surface moisture and temperature used in the present study have a maximum amplitude of 10 K and 4 K, respectively. The amplitude of the variation is deliberately conservative to match ABL equivalent potential temperature in the land case to the perturbation used in the ocean case.

2.4 The nonlinear switch and convective heating equations

Following [27], we use a nonlinear switch Λ which serves as a measure for the moistness and dryness of the middle troposphere. When the discrepancy between the boundary layer and the middle tropospheric equivalent potential temperature is larger than a threshold value θ^+ the atmosphere is defined as dry and the switch value is set to 1. Moist parcels rising from the boundary layer will have their moisture quickly diluted by entrainment of dry air, hence losing buoyancy and stop convecting, in such situations cumulus congestus clouds are favored. When this discrepancy is below some lower value, θ^-, the atmosphere is defined as moist and deep convection is favored. In this manner, the switch function can somehow be motivated based on a simple buoyancy mixing argument. A large difference between mid-tropospheric and boundary layer equivalent potential temperature leads to (horizontal) strong mixing of rising parcels, thus creating congestus clouds.

The function Λ is interpolated (linearly) between the two extreme values. Formally, the equation takes the form

$$\Lambda = \begin{cases} 1 & \text{if } \theta_{eb} - \theta_{em} > \theta^+ \\ A(\theta_{eb} - \theta_{em}) + B & \text{if } \theta^- \le \theta_{eb} - \theta_{em} \le \theta^+ \\ 0 & \text{if } \theta_{eb} - \theta_{em} \le \theta^-. \end{cases} \tag{19}$$

For the ocean case $\theta^+ = 20K$ and $\theta^- = 10K$ are chosen according to the Jordan sounding (Fig. 3.5 from [14]). For the land case, the value of $\triangle_m \bar{\theta}_e$ is lower due to the strong θ inversion (see Fig. 1). As described in [10], we lower the threshold values of $\triangle_m \theta_e$ that define the extremely dry and extremely moist limits by the amount of the inversion value, without disturbing the model physics. In the standard land case of 7.5 K inversion, we use $\theta^+ = 12.5$ K and $\theta^- = 2.5$ K. xw

The deep convective heating is obtained from a diagnostic equation

$$H_d = (1 - \Lambda) Q_d^+ \tag{20}$$

while the stratiform and congestus heating rates, H_s and H_c, solve relaxation type equations

$$\partial_t H_s = \frac{1}{\tau_s}(\alpha_s H_d - H_s) \tag{21}$$

$$\partial_t H_c = \frac{1}{\tau_c}(\alpha_c \Lambda Q_c^+ - H_c) \tag{22}$$

Aside of the nonlinear moisture switch the convective parameterization above take into account the convectively available potential energy (CAPE) available for both deep and congestus cumulus convection through terms Q_d and Q_c respectively.

The equation for deep convective heating is given by

$$Q_d = \bar{Q} + \tau_{conv}^{-1}[a_1\theta_{eb} + a_2 q - a_0(\theta_1 + \gamma_2\theta_2)]^+. \tag{23}$$

It has three main components. Deep convection is favored by the increase in θ_{eb} and q and decrease in $(\theta_1 + \gamma_2\theta_2)$. Thus, the convection is favored by increase in boundary layer moisture corresponding to CAPE parameterization and moist troposphere as in Betts-Miller type parameterization. Furthermore, colder middle troposphere facilitates deep convection by allowing saturation at weaker mixing ratios [27], through dry convective buoyancy parameter a_0. Meanwhile, the parameterization for bulk energy available for congestus clouds can be formally obtained by integrating over lower troposphere, the convective buoyancy anomaly of a dilute parcel raised from the boundary layer constantly mixing with the environment [28]. The equation takes the form,

$$Q_c = \bar{Q} + \tau_{conv}^{-1}[\theta_{eb} - a_0'(\theta_1 + \gamma_2'\theta_2)]^+. \tag{24}$$

Note that Q_c does not depend on vertically integrated atmospheric moisture and is driven by the boundary layer. Furthermore, Q_c has high sensitivity to the second baroclinic potential temperature through high value of $\gamma_2' = 2$ [28]. This reflects the sensitivity of congestus clouds to the variation in the lower tropospheric temperature, the region where the congestus clouds are most active.

Both the KM and the WK models share the convective parameterization presented in this subsection. The KM model as described above is used for linear analysis in section 3 and nonlinear simulations in section 4. Both the KM and the WK models in the above form are also used in [9] and [10] to study the diurnal cycle over the ocean and over land, respectively.

2.5 Reduced models for the diurnal cycle of precipitation

In this section, we derive the reduced version of the WK and the KM models that are capable of reproducing the essential features of the diurnal cycle of tropical precipitation. The study is carried out in the column framework where the spatial dependence is disregarded and velocity equations are omitted. This simplification is fully supported by the findings of [9,10] which show that the velocity component of the diurnal cycle accounts for very small part of the variability of the solution. Indeed, as discussed in [10], the resulting precipitation profiles of the full models and column approximations are nearly identical. However, unlike [10], we further eliminate the second baroclinic mode of the multicloud models. A similar procedure is used in [26] to elucidate the relationship between the multicloud parametrization with crude vertical resolution and other simpler model parametrizations in various limiting regimes. The resulting boundary value problem is solved by the standard BVP method of Matlab as described in [9].

We eliminate the second baroclinic mode from active dynamics by setting α_2, γ_2 and γ_2' to zero. Consequently, the mid tropospheric potential and equivalent potential temperature are reduced to

$$\theta_m = q + \frac{2\sqrt{2}}{\pi}\theta_1, \quad \text{and} \quad \theta_{em} = q + \frac{2\sqrt{2}}{\pi}\theta_1, \tag{25}$$

respectively. Further, the bulk energy available for deep and congestus convection loose the second baroclinic mode dependency.

The parameters ξ_c and ξ_s which control the contribution of the congestus and stratiform rain to the precipitation are set to zero, yielding $P = (2\sqrt{2}/\pi)H_d$. Lastly, the contribution of the congestus and

Table 1 Common constants and parameters for the WK and KM models.

Parameter	Value	Description
h_b / H_T /δ	500 m /16 km/ 0.03125	ABL depth/ Free troposphere depth/ratio of h_b to H_T
Q_{R1}	1 K/day	First baroclinic radiative cooling rate
Q_{R2}	Determined at RCE	Second baroclinic radiative cooling rate
Q_{Rb}	Determined By RCE	Boundary layer radiative cooling rate
ξ_s / ξ_c	0.5/1.25	Stratiform/Congestus contribution to first baroclinic mode
$\tilde{Q}$ / $\tilde{Q}_0$	0.9/ 6.5	Background moisture stratification/contribution to barotropic vertical moisture advection
$\tilde{\lambda}$ / $\tilde{\alpha}$	0.8/0.1	Coefficient of u_2 in linear / nonlinear moisture convergence
m_0	Determined at RCE	Large-scale background downdraft velocity
μ	0.25	Contribution of convective downdrafts to M_d
α_s / α_c	0.25/ 0.1	Stratiform/Congestus adjustment coefficient
α_m	0.2	Ratio of downdraft velocity (M_d) to upward mass flux velocity (M_u) at top of ABL
τ_R / τ_D	75 days / 50 days	Rayleigh drag / Newtonian cooling time scale
τ_s / τ_c	3 hours / 1 hour	Stratiform /Congestus adjustment time scale
τ_{conv}	2 hours	Convective time scale
τ_e	Determined by RCE	Surface evaporation time scale
τ_T	8 hours	Momentum entrainment time scale
$\bar{Q}$	Determined at RCE	Bulk convective heating at RCE
a_1 / a_2	0.45/0.55	Relative contribution of θ_{eb} / q to deep convection
a_0 / a_0'	7 / 1.5	Dry convective buoyancy freq. in deep/congestus eq.
γ_2 / γ_2'	0.1 / 2	Relative contribution of θ_2 to deep /congestus heating
α_2	0.1	Relative contribution of θ_2 to θ_{em}
κ	2	Ratio of q_t to q
C_d	0.001	Surface drag coefficient
u_0	2 m/s	Strength of turbulent fluctuations in the multicloud models

stratiform cloud to the downdrafts is suppressed by setting parameter $\mu = 0$ in (11). For the reader's convenience, the equations and closures for reduced KM and WK parameterizations are listed in table 2.

For the ocean case, the discrepancy between ABL equivalent potential temperature and mid tropospheric temperature is set to 12 K for both the KM and the WK models. In the WK model, we also impose a 5 K drop in moisture at the top of the ABL ($\triangle_t q = 5K$), while the potential temperature remains continuous throughout the atmosphere ($\triangle_t \theta = 0$). These parameters are identical to the ones used in the [9] and yield qualitatively similar RCE states, despite the neglect of the second baroclinic mode in the reduced models.

Figs. 2 and 3 present the resulting stable diurnal solutions of the one vertical mode resolution KM and WK models, in the ocean regime. Similarly to [9], the modeled diurnal cycle of precipitation is divided into four cyclic phases: 1) a CAPE (re)generation phase characterized by the enhancement of the boundary layer θ_{eb} flux during midday and early afternoon is followed by 2) a (re)moistening phase during the late afternoon, associated with lack of precipitation and radiative cooling that lasts until midnight. 3) Deep convection is initiated around midnight when the mid-troposphere is sufficiently moist and cool and (re)establishes the precipitation level near its radiative convective equilibrium (1 K Day^{-1}) and then 4) peaks with sunrise at 0600 LST to yield a precipitation maximum of roughly 2 K Day $^{-1}$ at around 1000 LST that dries the troposphere, consumes CAPE and thus closes the cycle.

The difference between the results of the full and reduced models, in ocean case, can be surmised by comparing Figs 2 and 3 to Figs. 2 and 3 of [9]. Since the reduced models lack the stratiform clouds, which lag deep convection in the full model, the reduced models exhibit more abrupt precipitation shutdown in the afternoon. In the case of the reduced KM model, this is compensated by a slightly longer period of afternoon deep convective precipitation and larger maximum. Furthermore, the moistening from the evaporation of stratiform rain is also not captured by the reduced model. As the result, the atmosphere takes longer to (re)moisten and morning cycle of deep convection is initiated late. In the case of the

Table 2 Prognostic and diagnostic equations for reduced KM and WK models. See text and Table 1 for details.

Name	reduced KM model	reduced WK model
Potential temperature, 1st mode	$\frac{\partial\theta_1}{\partial t} = H_d + S_1$	$\frac{\partial\theta_1}{\partial t} = H_d + S_1 + \frac{\pi}{2\sqrt{2}}E_{\alpha\beta}$
Radiative cooling	$S_i = -Q^0_{R,i} - \tau_D^{-1}\theta_i$	same
Sensible heat mixing flux	-	$E_{\alpha\beta} = \alpha\frac{E}{H_T}\triangle_t\theta + \beta(\frac{M_d}{H_T})\triangle_m\theta$
Free tropospheric moisture	$\frac{\partial q}{\partial t} = -\frac{2\sqrt{2}}{\pi}H_d + \frac{D}{H_T}$	$\frac{\partial q}{\partial t} = -\frac{2\sqrt{2}}{\pi}H_d + \frac{E}{H_T}\triangle_t q + \frac{M_d}{H_t}\triangle_m q + \frac{E}{H_T}\triangle_t\theta + \frac{M_d}{H_T}\triangle_m\theta - E_{\alpha\beta}$
Boundary layer equivalent potential temperature	$\frac{\partial\theta_{eb}}{\partial t} - = \frac{1}{h_b}(E_v - D)$	None
Boundary layer potential temperature	None	$\frac{\partial\theta_b}{\partial t} = -\frac{E}{h_b}\triangle_t\theta - \frac{M_d}{h_b}\triangle_m\theta + \frac{1}{\tau_e}\triangle_s\theta - Q_{Rb}$
Boundary layer moisture	None	$\frac{\partial q_b}{\partial t} = -\frac{E}{h_b}\triangle_t q - \frac{M_d}{h_b}\triangle_m q + \frac{1}{\tau_e}\triangle_s q$
Deep convection	$H_d = (1-\Lambda)Q_d^+$	Same
Maximum energy available for deep convection	$Q_d = \bar{Q} + \tau_{conv}^{-1}[a_1\theta_{eb} + a_2 q - a_0\theta_1]^+$	Same
Downdrafts	$D_c = m_0\triangle_m\theta_e$	$M_d = D_c$
Scalar entrainment velocity	None	$E = (M_u - M_d)^+$
Sea surface evaporation flux	$\frac{E_v}{h_b} = \tau_e^{-1}(\theta^*_{eb} - \theta_{eb})$	none

reduced WK model, the reinitiating of deep convection is less abrupt. Another cause contributing to the same effect is the lack of congestus heating, since in the full multicloud models, afternoon congestus clouds contributed to (re)moistening of the atmosphere prior to the deep convection. The simplicity of the models may not warrant a detailed comparison with observations, although overall the reduced and full models are qualitatively consistent with observations of the tropical precipitation over the oceans [63,64,31,45].

For the land case, the discrepancy between ABL equivalent potential temperature and mid tropospheric temperature is equivalent of 14K, in the WK model. As the land atmosphere is thought to have a somewhat drier mean state compared to the ocean scenario. As in [10], we also specify the 5 K drop in moisture at the top of the ABL ($\triangle_t q = 5K$). The RCE value of the flux of the potential temperature on top of the ABL is used to mimic the inversion and consequently we set $\triangle_t\theta = -7.5$ K. Thus potential temperature sharply raises at the top of ABL. Parcels raising to the top of the ABL suddenly encounter significantly warmer air, become negatively buoyant and sink back down. Other parameters used in the land case are identical to the ones used in [10] and yield a qualitatively similar RCE state. The sensitivity of the WK model to strength of the inversion and dryness of mean state is documented in [10].

Similarly to [10], the modeled diurnal cycle over land can be divided into a cycle of five phases: 1) an overnight phase of a radiative–convective equilibrium (RCE) state between 2000 and 0600 LST; 2) an early morning CAPE buildup accompanied by a sudden rise in precipitation that quickly dries and warms the middle troposphere occurs between 0600 and roughly 1000 LST, it is accompanied by

Table 3 Constants and parameters for MS01a and MS01b models

Parameter	Value	Description
$h_b/H_m/H/H_T/$	0.5 /5 /8/10 km	Height of ABL/middle-level troposphere / avg deep conv. /troposphere
u_0	5 m/s	Strength of turbulent fluctuations
C_θ^0	1.2×10^{-3}	surface-flux rate by wind
Q_{R0}	1 K/day	First baroclinic radiative cooling rate
C_D^0	10^{-3}	surface heating coefficient
N^2	$10^{-4}s^{-2}$	Brunt-Vaisala frequency
ϵ	0.1	strength of temperature fluctuations in ABL
θ_0	300K	temperature at top of ABL
θ_{eb}^*	10K	size of fluctuations in ABL most potential temp
$\theta_{eb} - \theta_{em}$	$\approx$ 20K	ABL and Mid trop temp discrepancy
Λ	0.9	Precipitation efficiency
Γ_m	6×10^{-3} K m^{-1}	moist lapse rate
γ	1.7	ratio of moist and dry lapse rates
τ_R/τ_D	75 days / 50 days	Rayleigh drag / Newtonian cooling time scale
τ_s/s	0.25/0.25	Stratiform heating time scale /fraction
μ	0.5	relative strength of stratiform downdraft
α_2	0.1	Dry convective buoyancy freq. in deep/congestus eq.
γ_2/γ_2'	0.1 / 2	Relative contribution of θ_2 to deep /congestus heating
α_2	0.1	weight of second baroclinic mode heating in CAPE

the entrainment of ABL sensible heat flux into the free troposphere which facilitates further warming and eventually results in a shutdown of precipitation; 3) a moistening/radiative cooling phase between roughly 1000 and 1600 LST; 4) a phase of maximum precipitation between 1600 and 1800 LST that dries the middle troposphere and quickly consumes CAPE; and 5) remoistening phase that restores the moisture level to sustain the overnight RCE precipitation and connects to phase 1 in the cycle. As in the ocean case, precipitation profiles of full and reduced models are qualitatively similar (as can be seen by comparing Fig. 4 to Fig. 2 of [10]). The lack of moistening by evaporation of stratiform rain and moisture convergence produces minor differences in the timing of deep precipitation and rapidness of the remoistening phases.

In both land and ocean cases, the lack of the second baroclinic mode does not impede the reproduction of the diurnal cycle of precipitation. While no congestus clouds are produced, the enhanced boundary layer flux produces artificial drying of the troposphere and thereby drives the nonlinear switch to reduce deep convective precipitation.

2.6 A diurnal cycle in simplified mass flux parameterizations

While the nonlinear switch that determines the amount of congestus and deep convective clouds is a crucial feature of the multicloud model, it is interesting to consider diurnal solutions of a more conventional mass flux parameterization. Simple crude vertical resolution models were at the forefront of theoretical efforts in understanding convectively coupled waves and MJO[8,44,65,40]. Here we confine our study of diurnal cycle to Majda Shefter models [37,36] (hereafter MS01a and MS01b) .

MS01a is a single baroclinic mode model for deep convection. As in the multicloud model, two layers represent the atmosphere. The boundary layer is driven by the evaporation from the sea surface while radiative cooling is imposed in the free troposphere. In the column model setting, the MS01a reduces to an equation for the first baroclinic mode of potential temperature supplemented by an equation for mid-tropospheric equivalent potential temperature.

$$(1 - \sigma_c)\frac{\partial \theta_1}{\partial t} = H_d - S_1 \tag{26}$$

$$\frac{\partial \theta_{em}}{\partial t} = D/H - Q_R \tag{27}$$

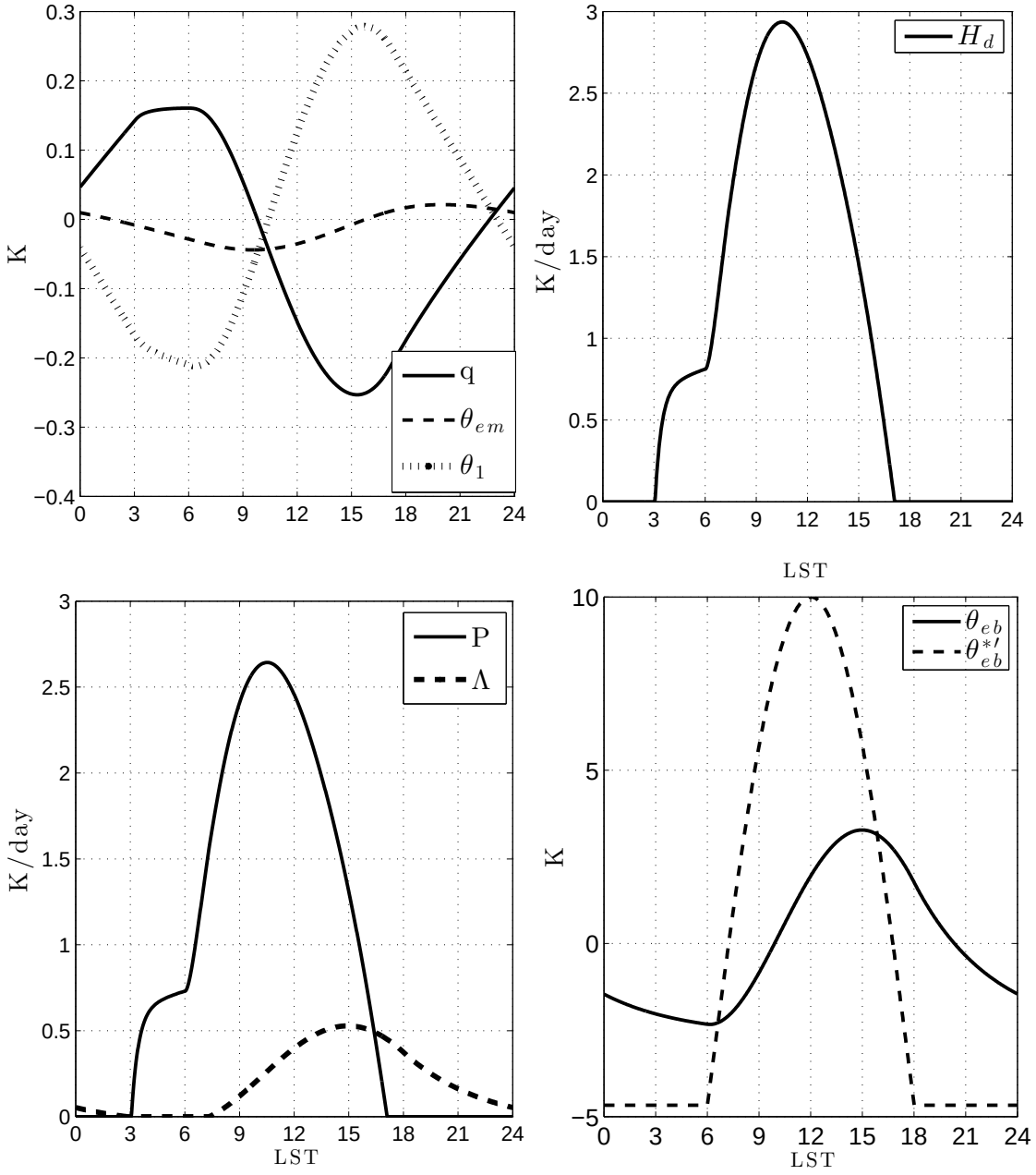

Fig. 2 Stable periodic response of the reduced KM model to a diurnal cycle forcing in the ocean regime.

A constant the area fraction of deep convection, σ_c, is used for the convective parameterization closure. In this study, the fraction is fixed to 0.01, which is one of the typical values used in [37]. The deep convective heating is proportional to the product of σ_c and convective updraft velocity w_c:

$$H_d = \frac{\bar{\alpha}}{H_m}\sigma_c w_c. \tag{28}$$

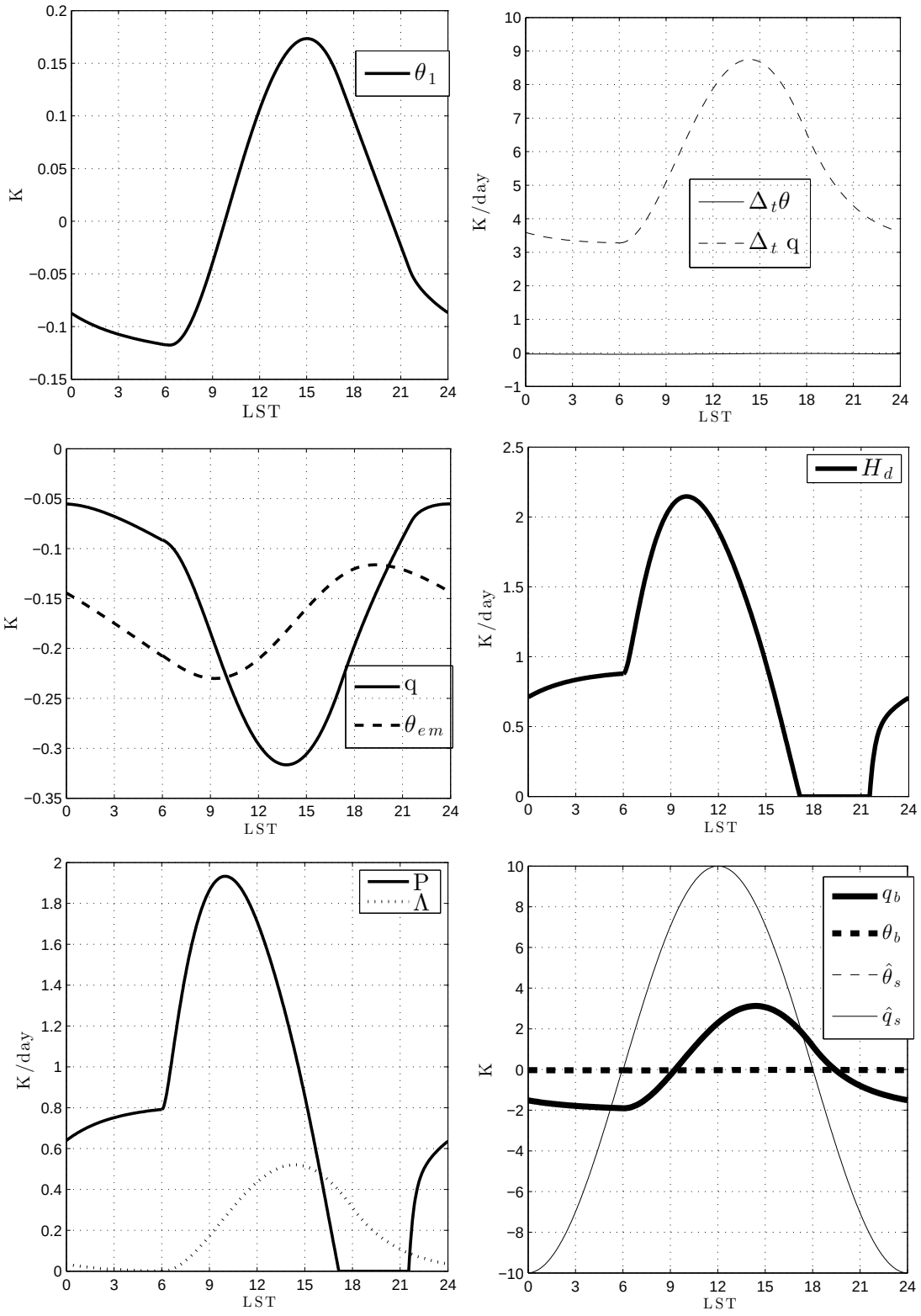

Fig. 3 Stable periodic response of the reduced WK model to a diurnal cycle forcing in the ocean regime.

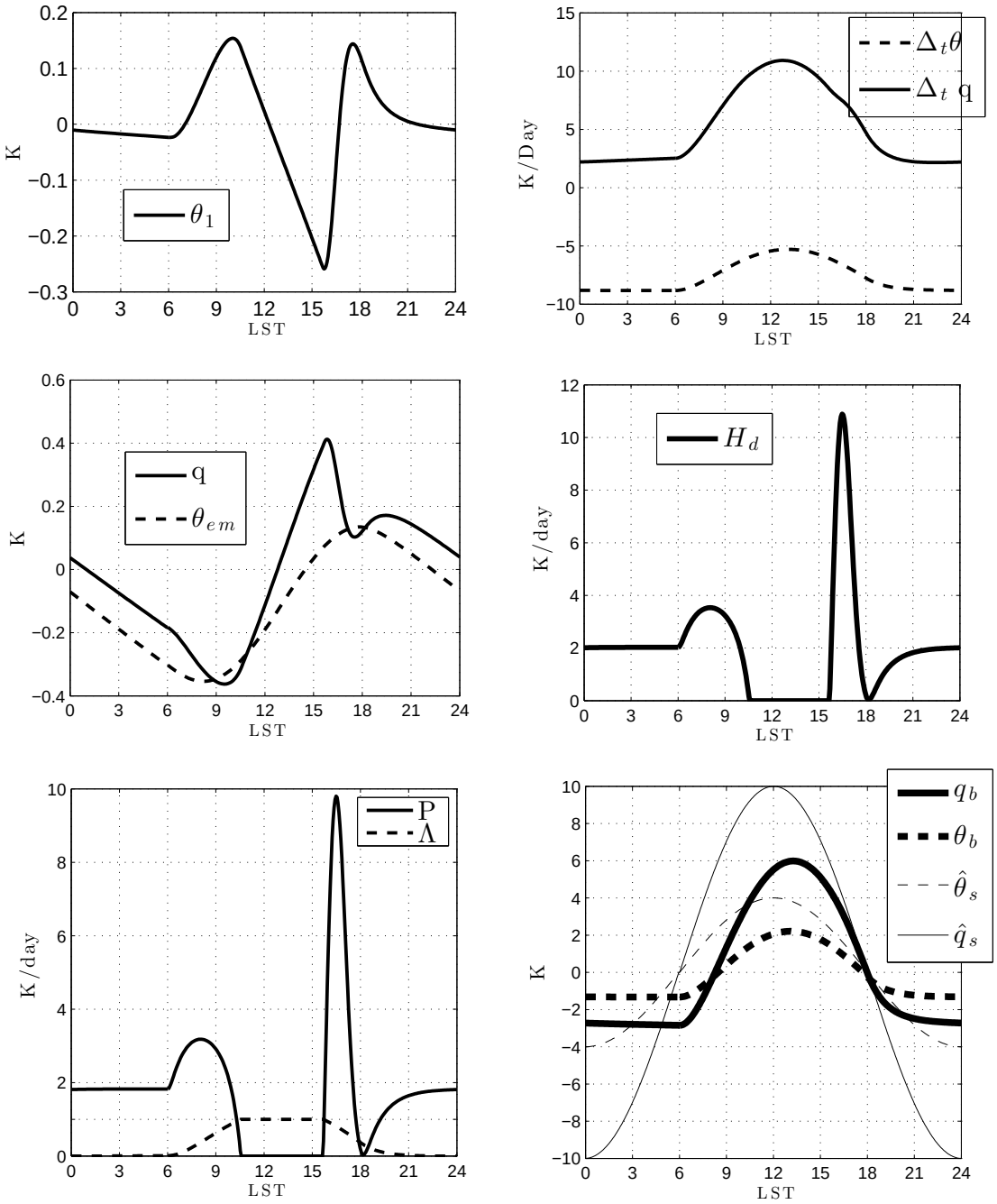

Fig. 4 Stable periodic response of the reduced WK model to a diurnal cycle forcing in the land regime

While, many parameterizations of convective updrafts are considered in [37], here we assume fluctuations in CAPE are instantaneous balanced by the kinetic energy of the convective updraft. Leading to algebraic expression for the convective updraft:

$$w_c^2 = \frac{c_p H_m}{2\theta_0 H}(\theta_{eb} - \gamma\theta) \tag{29}$$

This, aptly named, ICAPE closure is derived from the Lagrangian parcel adjustment (LPA) scheme [65, 66] and like LPA it has a finite band of instability when wind induced surface heat exchange (WISHE) is allowed. However, the ICAPE closure avoids the nonphysical parasitic waves associated with LPA scheme [37,36].

The free troposphere communicates with the boundary layer through downdraft D, given by

$$D = -[(1-\sigma_c)w_e^- - \sigma_c w_d](\theta_{eb} - \theta_{em}). \tag{30}$$

Here, $w_e = -\sigma_c/(1-\sigma_c)w_c \approx -\sigma_c w_c$ is the speed of compensating environmental descent, in this column model setting, and w_d is convective downdraft. The equation for convective downdraft is given by

$$w_d = \frac{1-\epsilon_p}{\epsilon_p} w_c, \tag{31}$$

with the precipitation efficiency, $\epsilon_p = 0.9$. The closure for the boundary layer evaporation is nearly identical to the one used in the multicloud model. Namely, we set $E_v = C_\theta^0 u_0(\theta_{eb}^* - \theta_{em})$, where the constant u_0 is the typical size of the turbulent velocity fluctuations. However, we note that the full MS01a model includes the contribution to surface drag from the mean flow and the first baroclinic mode of velocity fluctuation. To compensate for the lack of mean flow (in the model that utilizes wind induced surface heat exchange mechanism), we increase the turbulent drag coefficient u_0 from 2 m/s (as used in MS01a) to 5 m s^{-1}. This is the only significant change from the parameters used in [37]. Equations (26) to (31) form the single column version of the MS01a model.

A logical extension of the MS01a is the model for stratiform instability (MS01b) introduced in [36]. Here, the dynamical core consists of the first two baroclinic modes of the primitive equations, just like in the full multicloud models [27,29,58].

$$\frac{\partial \theta_1}{\partial t} = H_d + S_i', \qquad \frac{\partial \theta_2}{\partial t} = H_s + S_i' \tag{32}$$

$$S_1' = \frac{1}{1+s}Q_{R1} - \frac{1}{1+s}\frac{\theta_1}{\tau_R} \qquad S_2' = \frac{s}{1+s}Q_{R1} - \frac{s}{1+s}\frac{\theta_2}{\tau_R} \tag{33}$$

The stratiform heating is not explicitly present in the first baroclinic mode and thus the deep convection heating is still given by (28). The convective updraft is closed by

$$w_c^2 = \frac{c_p H_m}{2\theta_0 H}(\theta_{eb} - \gamma\theta_1 - \alpha_2\gamma\theta_2) \tag{34}$$

where α_2 is a constant parameter that allows a second baroclinic mode contribution to CAPE. Similar to the multicloud model, the stratiform heating satisfies a relaxation-type equation.

$$\frac{\partial H_s}{\partial t} = \frac{1}{\tau_s}(\alpha_s H_d - H_s) \tag{35}$$

The downdraft from the evaporation of stratiform rain is included in the environmental downdrafts to produce $w_e = -\sigma_c w_c - \frac{\alpha_2 H_m}{\bar{\alpha}} H_s$. Similarly to MS01a, the convective downdraft is given by

$$\sigma_c w_d = \frac{1-\epsilon_p}{\epsilon_p}((1-\mu)\sigma_c w_c + \mu\frac{H_m}{\bar{\alpha}} H_s s^{-1}) \tag{36}$$

The equations (32)–(36) and boundary layer equation (28) fully describe the MS01b model. In MS01b, the dynamical equation for θ_{em} is replaced by the RCE value in MS01a model. It is easy to see that when $\alpha_s = \mu = \alpha_2 = 0$, MS01b reduces to MS01a.

Fig. 5 presents the diurnal cycle solutions obtained from the MS01a and MS01b models. The resulting solutions have peaks in precipitation that resembles in structure the SST forcing perturbation. The precipitation starts at 0600 in the morning and peaks around noon. The diurnal cycle in both the MS01a and MS01b models can be split into three phases: 1) a morning phase characterized by enhancement of the boundary layer flux, (re)generation of CAPE and instantaneous warming of the atmosphere by the compensating updraft; 2) a phase of afternoon cooling of the atmosphere; 3) an overnight suppressed convection phase associated with diminished boundary layer flux and thus lack

of CAPE. In the case of MS01b, the addition of stratiform clouds does little aside of smoothing the shape of the afternoon precipitation. This results in a 15-minute delay of the convective maximum, which occurs at 1224 instead of 1210 in the MS01a model.

The MS01 models contain a number of tuning parameters. While the results are omitted, the variation of convective area fraction and precipitation efficiency parameters does not lead to qualitatively different outcome. In fact, a deviation from the parameters used in MS01a and MS01b publications often leads to states where the diurnal solution cannot be found. Furthermore, the narrow parameter range in which solutions can be found contains many unstable solutions.

2.7 The main physical features of the multicloud parameterization

The precipitation profiles for all models considered in this paper are plotted in the top of Fig. 6 along with those of the full KM and WK models in the corresponding parameter regimes. As noted above, the diurnal solutions of the reduced "multicloud" models are qualitatively similar to those of the full multicloud models and thus capture the main features of the diurnal cycle of precipitation in the tropics. The one and two baroclinic mode models MS01a and MS01b are also qualitatively similar to each other but they dramatically fail to capture the essential feature of the diurnal cycle of tropical precipitation over the ocean, namely, the early morning precipitation maximum (note that MS01 models were not tested in the land regime because the full boundary layer dynamic is developed only for the KM model, in [58]).

The main difference between the multicloud KM models and the MS01 models is the use of the nonlinear moisture switch that allows congestus preconditioning prior to deep convection. As in conventional GCM parameterizations, the MS01 models are based on a fixed convective area fraction σ_c and thus the structure of the precipitation is tied directly to CAPE. Precipitation is activated whenever CAPE is positive. The lack of the free tropospheric moisture in the MS01b parameterization is important but secondary effect. As shown in [9], the multicloud model produces qualitatively similar results when the moisture dependence is omitted from the CAPE closure. In the case of the MS models, boundary layer driven CAPE and fixed deep convective fraction amount to precipitation profiles that mirror the boundary layer fluxes.

While congestus clouds are absent from the reduced/one baroclinic mode KM and WK models, the nonlinear switch still responds to the artificial relative drying of the atmosphere by reducing deep convective heating. While no congestus clouds are produced, the enhanced boundary layer flux produces artificial drying of the troposphere and thereby drives the nonlinear switch to reduce deep convective precipitation. This implicit representation of congestus is exactly what allows the reduced multicloud model to reproduce the precipitation profile of the full model. The use of nonlinear switch in such one-column setting can be equated to the use of convective triggers [60,67,19,57]. The use of such triggers, in mass flux schemes, has been shown to increase convective variability overall and produce convectively coupled equatorial waves with enhanced congestus to deep to stratiform phase tilts and realistic phase speed [12].

Over the land, the reduced WK model reproduces the diurnal cycle that closely resembles the results of the full model. In this case, the essential physical mechanism at work is the direct entrainment of boundary layer sensible heat into the free troposphere. The sensitivity analysis to the sensible heat entrainment parameters α and β is presented on the bottom of Fig. 5. A larger entrainment parameter allows for faster warming of the atmosphere by the ABL sensible heat and thus produces more defined afternoon precipitation peak and diminishes the amplitude of the morning precipitation (through a raised value of the dry convective buoyancy frequency in the WK model).

However, the one baroclinic mode models are inherently limited in their usefulness. The second baroclinic mode structure provides the tilt of the convectively coupled waves (CCW). Aside of being and important observation feature, it is established in [36,27,28, etc.] that the second baroclinic mode plays an important role in determining the speed and scale selective instability of CCWs. The CCW tilt is important for convective momentum transport [42,4,35,38,39,23].

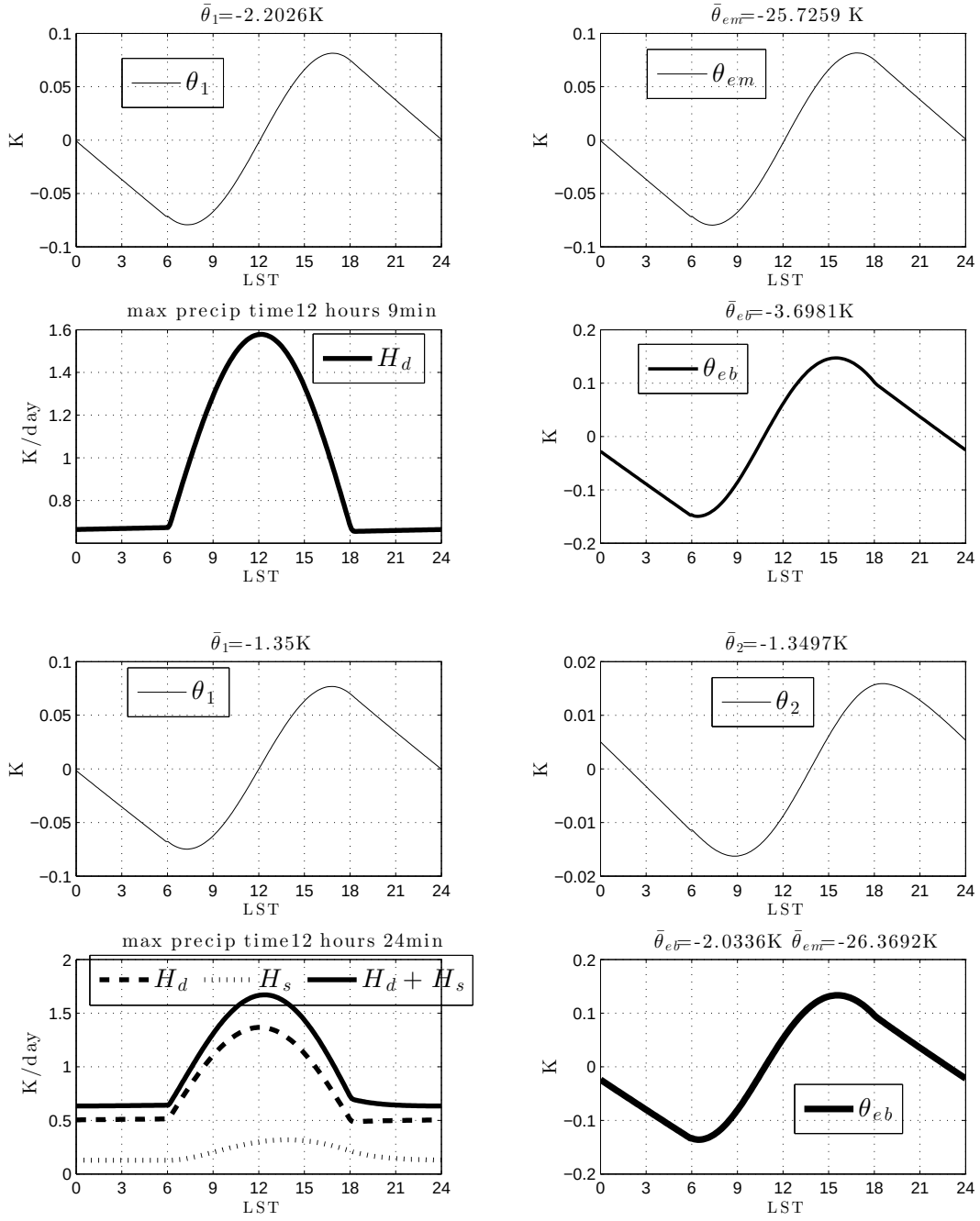

Fig. 5 Stable periodic response of the MS01a and MS01b, top and bottom four panels,respetively to a diurnal cycle forcing in the ocean regime.

3 Interaction of convectively coupled waves and the diurnal cycle

3.1 Linear stability

Linear stability analysis is a standard tool for understanding the behavior of convectively coupled waves. The procedure is straightforward and the interested reader is referred to [27,29] for further detail. First the dynamical model is linearized about an RCE state to obtain equations for the first-

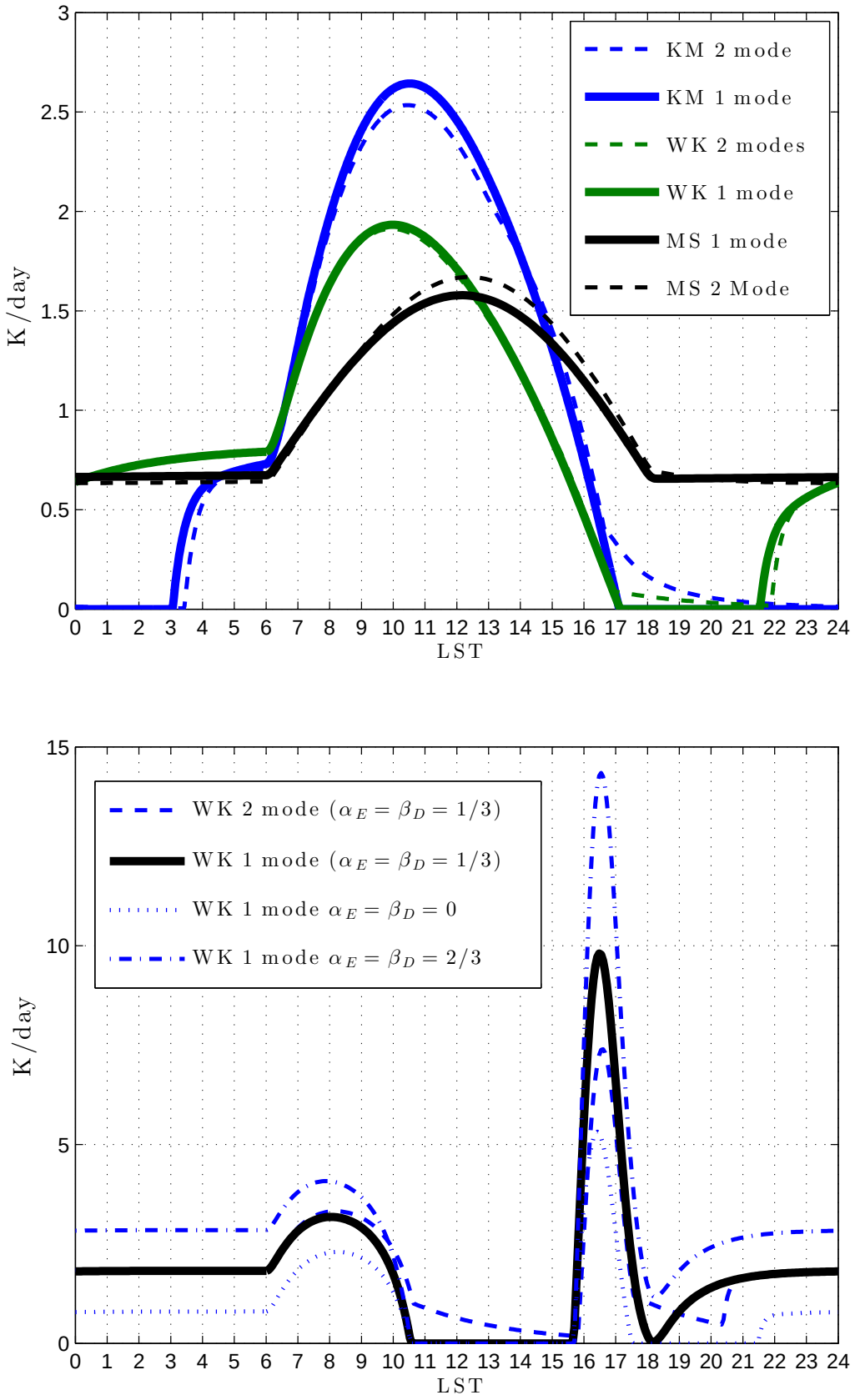

Fig. 6 Precipitation profiles of convective parameterizations in ocean regime (top) and precipitation profiles for land regime and sensitivity to entrainment parameters α_E, β_D(bottom).

order perturbations, $U(x,t) = (u_1, u_2, \theta_1, \theta_2, \theta_{eb}, q, H_s, H_c)$. We then look for traveling wave solutions of the form $U(x,t) = \hat{U}\exp[i(kx - \omega t)]$, where k is the wavenumber and $\omega = \omega(k)$ is the generalized dispersion relation. Here, $Re(\omega)/k$ is the phase speed and $Im(\omega)$ is the growth of the linear wave [37, 36].

In order to understand the impact of the diurnal cycle on convectively coupled waves, we recall that the diurnal cycle perturbation $\theta_{eb}{*}'$ adds up to 10 K to the constant background value of $\theta^*_{eb} - \theta_{eb} = 10$ K during day time. At night, the value of roughly 5 K is subtracted form the background state. Thus we consider linear stability analysis about RCEs where the "constant" $\theta^*_{eb} - \theta_{eb}$ takes values between 20 and 5K corresponding to the values of the surface flux around noon and nighttime as perturbations of the standard value of 10 K.

Fig. 7 presents the dispersion relation for the three extreme cases. The most interesting feature is a band of instability (highlighted by small circles in the phase plots) associated with the moisture coupled gravity waves. The region of highest growth is centered at wavenumber $k = 13$ for the standard case $\theta^*_{eb} - \theta_{eb} = 10$ K. Larger amount of latent heat flux during the day enhances the instability, while lower value of $\theta^*_{eb} - \theta_{eb}$ has the opposite effect. Thus the instability band expands during the day and shrinks at night favoring lower wavenumber modes. It should be noted that the growth rate as a function of wavenumber has the shape of an inverted parabola for all cases considered here. The interested reader is referred to [29] for more details about the linear analysis procedure and for an extensive parameter sensitivity analysis of the multicloud model.

The structure of the most unstable modes is plotted in the right column of Fig. 7. The linear stability analysis of the enhanced surface flux state reveals slower propagating and faster growing waves. During night, the wavenumber 10 mode has highest instability. However, if we were to limit our investigation to wavenumber 13 modes, we would note that the diminished nighttime flux increases the phase speed and damps the growth rate. Further, the boundary layer equivalent potential temperature θ_{eb} gains strength relatively to the mid-troposphere moisture q. The vertical structure of the most unstable modes in all three scenarios is characterized by a backward and upward tilt in wind and temperature fields. These modes, with propagation velocity of approximately 15 m/s, are similar to the moisture coupled waves presented in [27, 29].

The parameter regime used throughout this section deviates slightly from the ocean parameter regime presented in Section 2 and used in [9]. First, the value of dry convective buoyancy frequency is lowered from $a_0 = 7$ to $a_0 = 5$ in order to facilitate deep convection. Secondly, a slightly drier background profile, $\theta_{eb} - \theta_{em} = 14$ K (instead of $\theta_{eb} - \theta_{em} = 12$ K) is assumed in order to enable higher congestus heating, which strengthens the waves through the low level moisture convergence.

3.2 Nonlinear simulations

In this subsection, we perform numerical simulations with the full nonlinear KM multicloud model, described in (1) through (16). We solve these equations in (x,t) variables on a 40 000-km periodic ring representing the perimeter of the Earth at the equator. We use an operator time-splitting strategy that separates the purely hyperbolic system from the convective forcing terms of the right hand side that are treated as an ODE system [24, 25]. Three different forcings are considered: a case of constant surface fluxes without diurnal cycle (i.e $\theta^*_{eb}{}' = 0$ in (17)), a weak diurnal cycle forcing of 1.5 K maximum, and a strong diurnal cycle forcing of 10 K amplitude.

In the left column of Fig. 8 we show the contours in the space-time domain of the first and second baroclinic velocity, deep convective and congestus heating over the last 20 days of a 200 day simulation. The results show a wave train of six individual moisture coupled gravity waves moving eastward with a velocity of approximately 15 m s^{-1}. They have an average wavenumber 6, which is slightly smaller than the instability peak wavenumber $k = 13$, predicted by linear theory. Contrary to the physical intuition, this shift in wavenumber is not due to a shift in the basic state as the time-averaged solution (not shown) remains relatively homogeneous and identical to the imposed RCE solution [29]. The five day intensification decay cycle of the waves is brought about by strengthening and decay of the congestus heating field and the associated low level moisture convergence. Both the structure of the waves and organization of the wave train resemble the structures found in the explicit numerical simulations [15]. Moreover, the convective variability is reminiscent of tropical superclusters or convectively coupled Kelvin waves observed in nature[62, 61, 52]. The addition of a weak diurnal cycle perturbation to

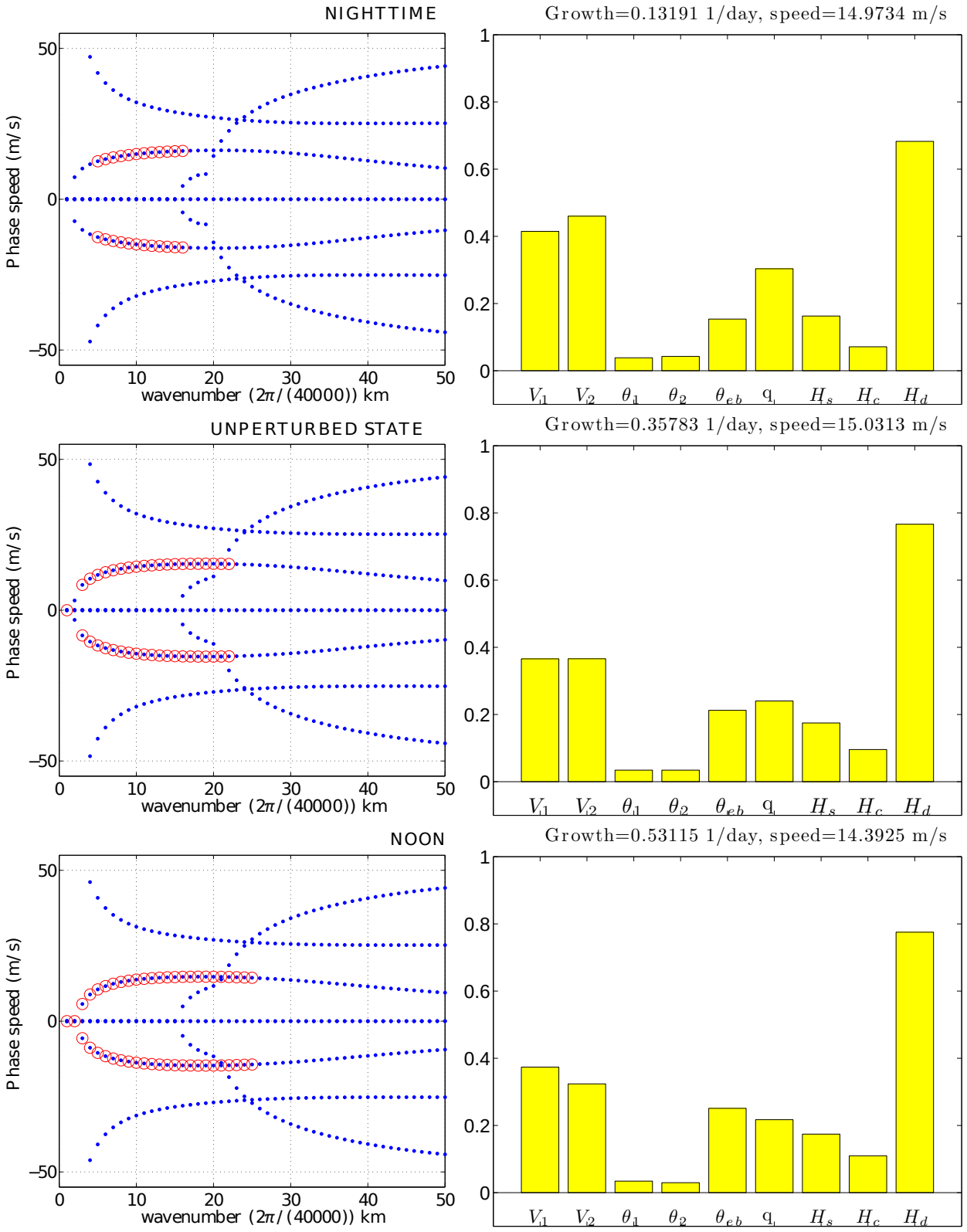

Fig. 7 Dispersion relations (left) and composition of the most unstable mode (right) for linear stability about RCE with $\theta^*_{eb} - \theta_{eb}$ fixed to 5K (top), 10K (middle) and 20K (bottom). The unstable modes are highlighted by small circles in the phase plots.

the nonlinear simulations leads to disintegration of the five-day intensification and decay cycle, as seen in the right column of Fig. 8. The diurnal boundary layer heating allows for a daily congestus preconditioning. This creates a weaker wavenumber 6 (on average) waves, traveling in a wave train eastward at approximately 15 m s^{-1}.

By using a 15 m s^{-1} eastward moving reference frame, we construct a composite of the moisture coupled gravity waves but averaging in "time" along this moving frame. The averaged solution is shown in Fig. 9 without and with weak diurnal cycle, respectively. In both cases, the waves have congestus to deep to stratiform heating pattern reminiscent of convectively coupled tropical waves [61,27,26]. Additional features include a backward and upward tilt in the wind and temperature fields, upper-tropospheric warm temperature anomalies slightly leading and/or within the region of upward motion, which is in phase with the heating anomalies, low-level convergence and congestus heating leading the wave, and an upper-tropospheric stratiform wake.

In the case of the strong diurnal cycle, Fig. 10, the convectively coupled waves disappear and the variability of the system becomes locked to the diurnal forcing. It is interesting to note that due to the periodicity of the domain, the periodic solution forms a standing wave pattern. Averaged in the LST reference frame, bottom of figure Fig. 10, the precipitation profile closely resembles the predictions of the analysis of [9].

3.3 Failure of the one baroclinic mode models to capture CCWs

It is possible to apply the same analysis to the reduced multicloud model. The reduced KM model, described by equations (1) – (16) is subject to the linear stability analysis. The only difference in parameter regime, as discussed in Section 2, is that parameters $\alpha_2, \gamma_2, \xi_s, \xi_c, \tilde{\gamma}, \tilde{\alpha}, \mu$ are all set to zero. As described in Section 2, this allows us to completely decouple the second baroclinic mode. Thus both linear analysis and nonlinear simulations involve a set of four equations for $U(x,t) = (u_1, \theta_1, \theta_{eb}, q)$ for which we utilized the numerical methods described and referenced above.

The results are presented in Fig. 11. The top two panels of the figure present the dispersion relations and the structure of the most unstable mode for $\theta^*_{eb} - \theta_{eb} = 10$ K as in our standard unperturbed RCE state. We note that the dispersion relation is fundamentally different from the structure of the dispersion relation of the full model. The most unstable mode is a weakly growing standing wave with no convective tilt and no propagation, thus fundamentally different from tropical superclusters. The results are very similar with $\theta^*_{eb} - \theta_{eb} = 5$ and 20 K and are omitted for brevity.

The nonlinear simulations show that these standing waves saturate to very small values, as seen in Fig.12. The standing wave weakly interacts with the diurnal cycle, whose effects are most obvious in the heating field. The forced one day amplification and decay cycle of the waves is an important result, which carries on, but both the structure of the waves and the small magnitude are not relevant to atmospheric science. The weakness of the waves is likely due to the absence of the strong low level moisture convergence associated with the congestus heating.

Thus while, one baroclinic mode model can reproduce diurnal cycle over land and ocean, it fails to adequately capture convectively coupled waves. The fundamental difficulty resides in the inability of one baroclinic mode models to capture the tilt of the waves. Aside of being important observational feature, the tilt of the CCWs is believed to be responsible for the propagation and reinforcement of the moisture coupled waves via the congestus preconditioning in front of the wave and the stratiform downdrafts in its wake [36,27,29].

4 Concluding discussion

The multicloud model [27,28,58] is used here to study the diurnal cycle of tropical precipitation over the ocean and over land. The full model consists of the first two vertical baroclinic modes of vertical structure forced by heating profiles based on the three cloud types that characterize organized tropical convection: cumulus congestus, deep convection, and trailing stratiform cloud decks, coupled to a thin boundary layer that responds to solar surface heating and downdrafts. The reduced models are derived by eliminating the second baroclinic mode of the vertical structure. In the context of the multicloud framework, we study two important questions: 1) What is the minimal model that can be used to

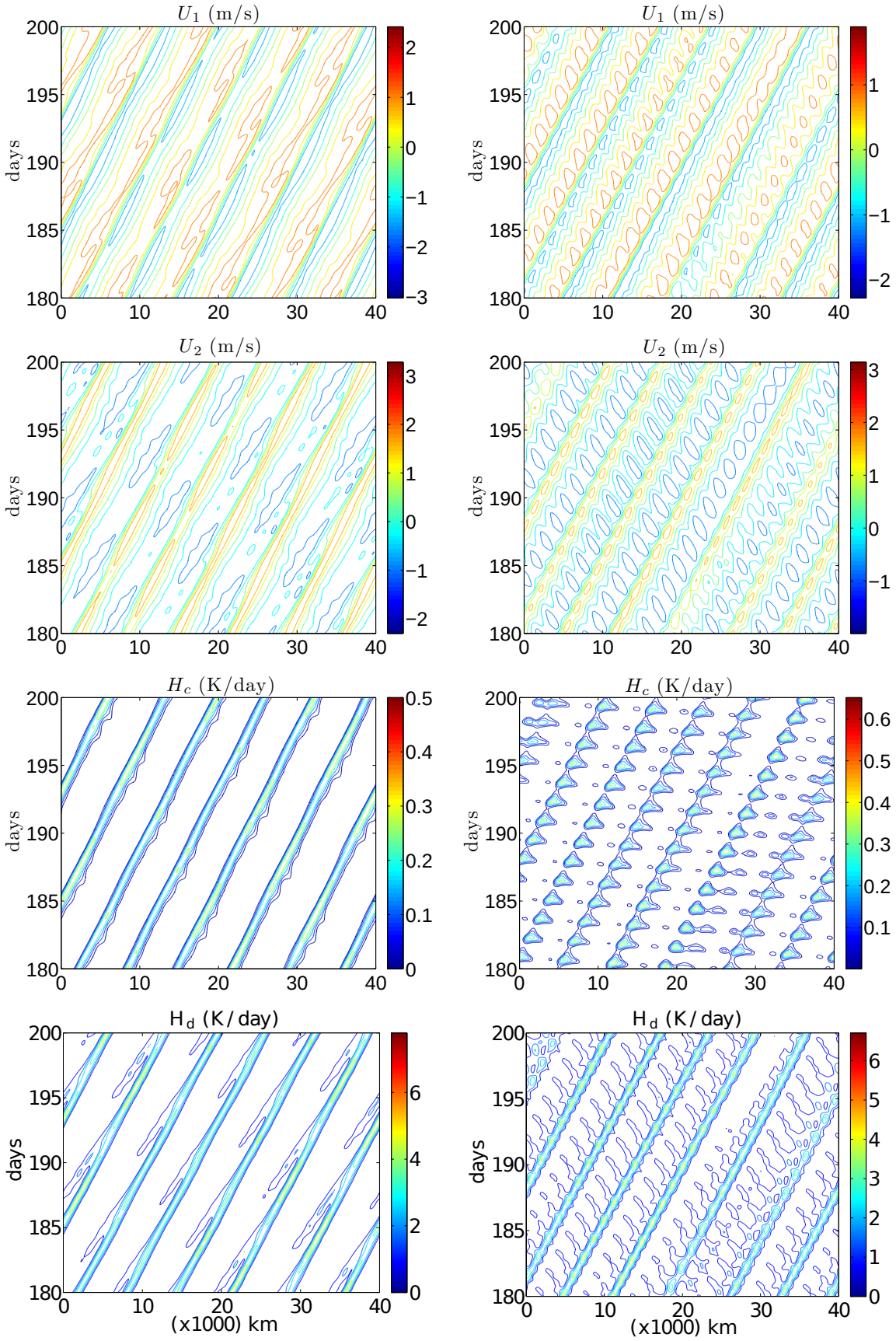

Fig. 8 Plot of $x - t$ contours of 1st and 2nd baroclinic velocity, deep and congestus convective heating fields over the last 20 days of full KM model simulations, without (left) and with (right) diurnal cycle.

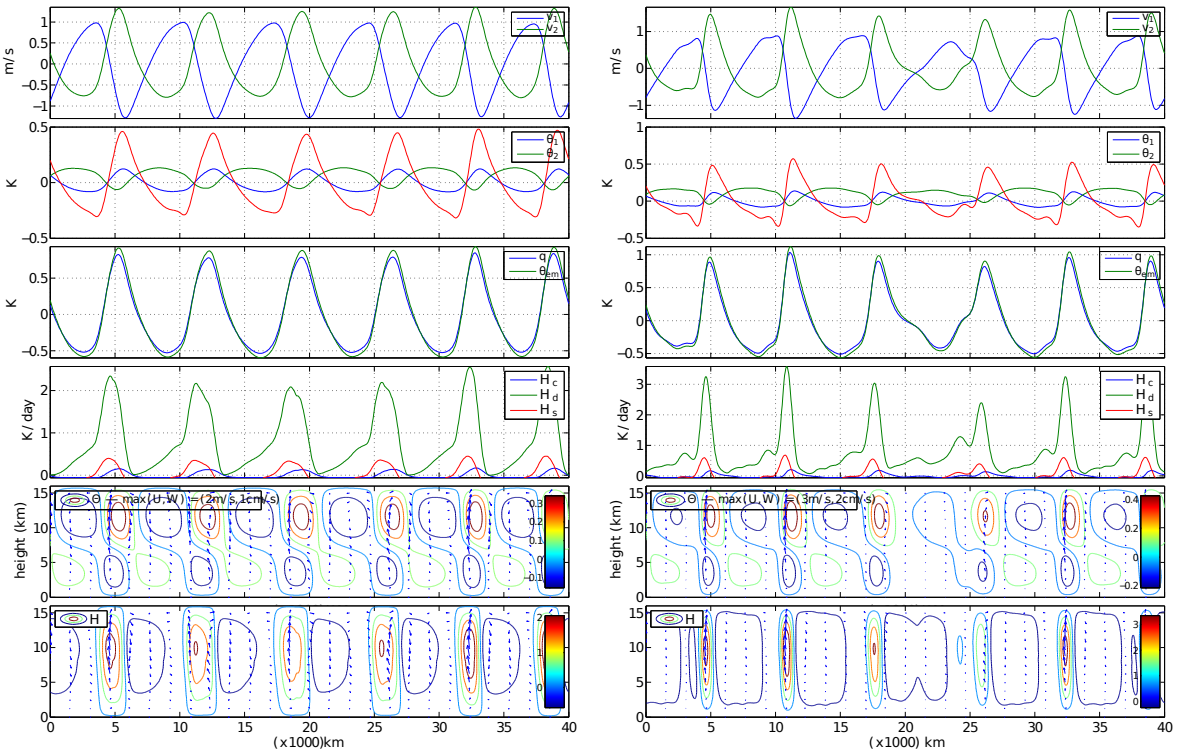

Fig. 9 Average in a 14 m s^{-1} eastward moving reference frame of the dynamic variables and heating fields for nonlinear simulations without (left) and with (right) diurnal cycle

model the effects of diurnal cycle over land and ocean? 2) What is the minimal model necessary for understanding the interactions of the diurnal cycle with the CCWs?

The one baroclinic mode version of the multicloud model is found to be the answer to the first question. It is found here that a one baroclinic mode model, supporting only one cloud type, deep convection, is sufficient for capturing the diurnal cycle over land and over the ocean, provided a moisture switch function is used as surrogate for congestus preconditioning. The reduced multicloud model can successfully capture the main qualitative features of the diurnal cycle over land and ocean, namely, the morning precipitation over the ocean and a sharp afternoon precipitation maximum over land, mimicking the results of the full multicloud model. As discussed in Section 2, the skill of the reduced model in capturing the diurnal cycle is fundamentally linked to the use of nonlinear switch function that allows the reduced model to mimics the congestus preconditioning mechanism of the full multicloud models. It is further shown that a mass flux parameterization, which relies solely on a fixed deep convection fraction, fails to capture the diurnal variability.

The interaction of the diurnal cycle with convectively coupled waves is described through linear analysis and nonlinear simulations on the equatorial ring. In the full model, the moist gravity waves with an average wavenumber 6 and phase speed of approximately 15 m s^{-1} readily interact with a weak diurnal cycle. Nevertheless, a strong diurnal cycle leads to a purely diurnal solution that is locked to the surface fluxes. Both scenarios are observed in nature, though not on planetary scale [3]. The one baroclinic mode model fails to produce physically relevant waves in the same parameter regime. Thus the two baroclinic mode model is necessary for the study of CCWs and their interactions with the diurnal cycle.

Acknowledgements The research of B. K. is supported by a grant from the Natural Sciences and Engineering Research Council of Canada. The research of A.J.M. is partially supported by National Science Foundation grants DMS-0456713 and DMS-1025468, and the office of Naval Research (ONR) grants DRI N0014-10-1-0554 and N00014-11-1-0306. Y.F. is supported as a postdoctoral fellow on the latter ONR grant.

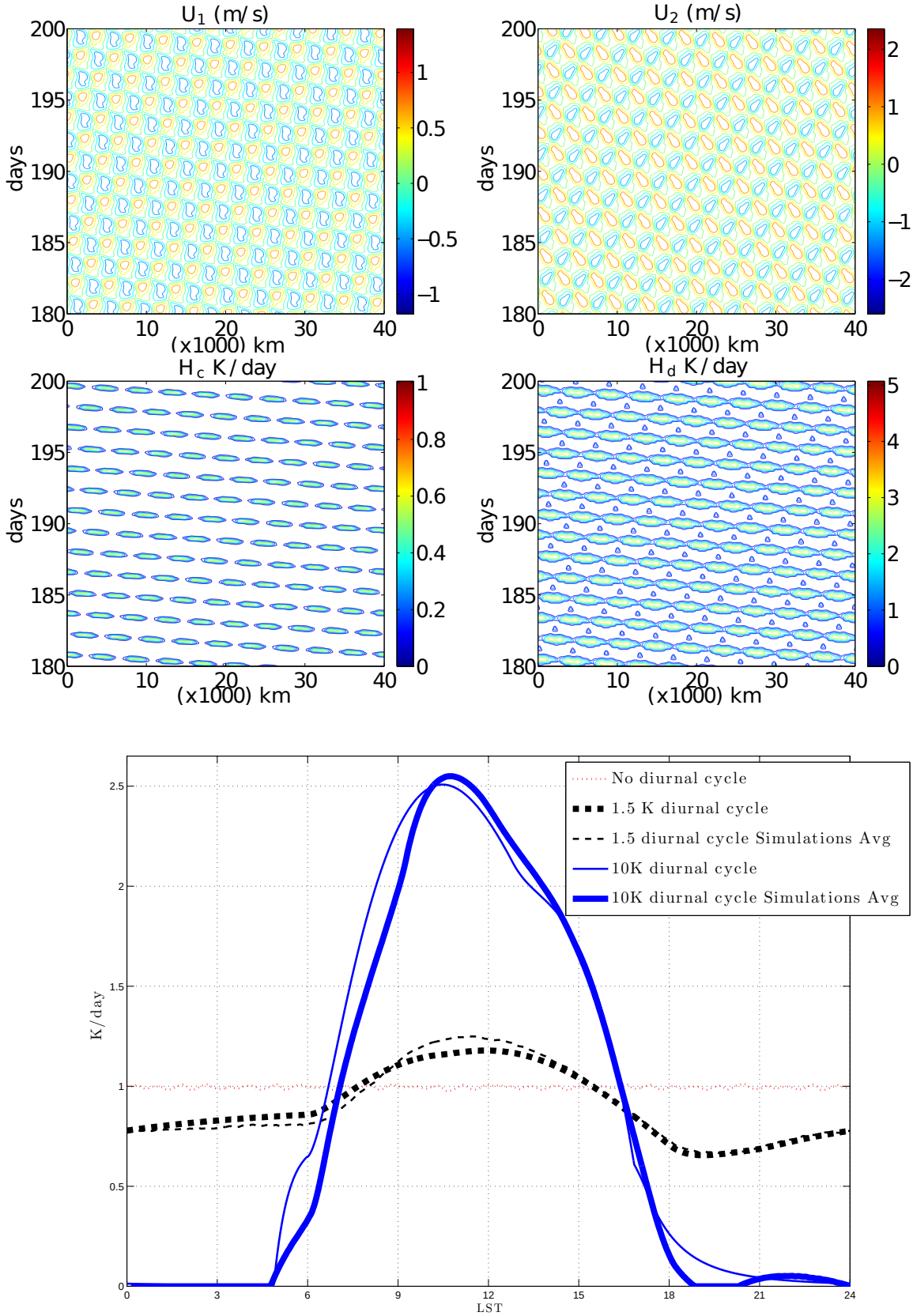

Fig. 10 Plot of $x-t$ contours of 1st and 2nd baroclinic velocity, deep and congestus convective heating fields over the last 20 days of full KM model simulations with strong diurnal cycle (top four panels). Bottom panel corresponds to the LST average of precipitation from the simulations with and without diurnal cycle. Here thin lines denote solutions obtained by solving BVP [9]

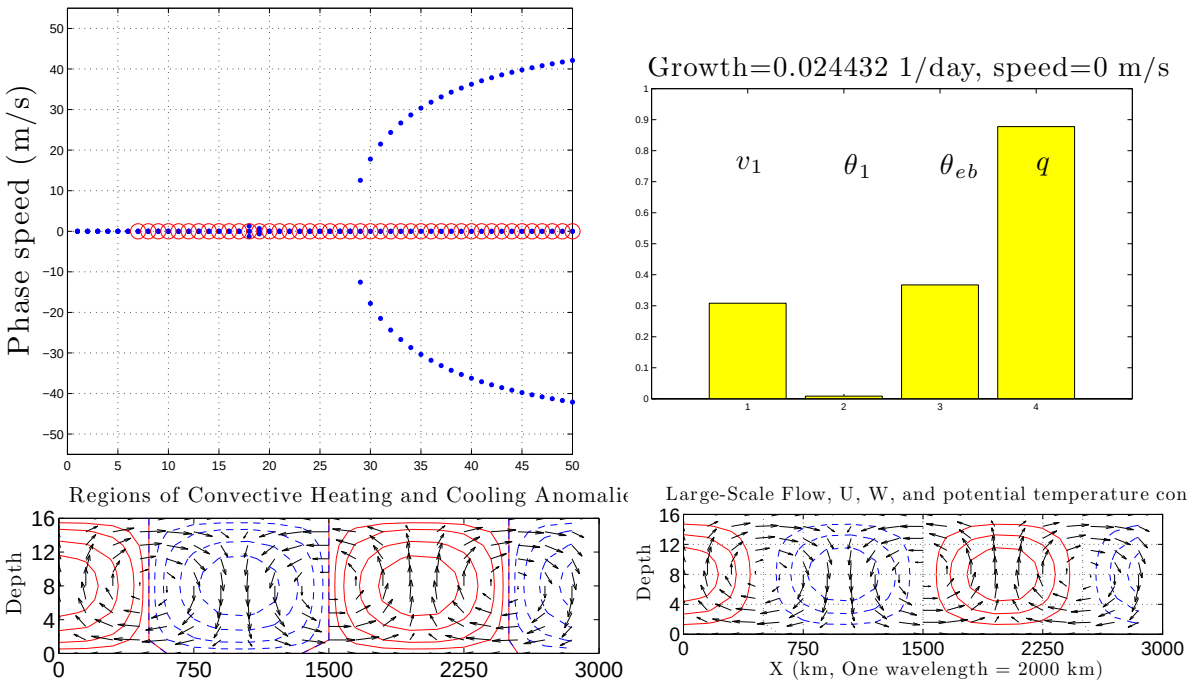

Fig. 11 Dispersion relation (top left), structure of the most unstable mode (top right) and structure of heating and velocity fields (top left and right, respectively) from the linear analysis of reduced KM model

References

1. Albright, M.D., Mock, D.R., Recker, E.E., Reed, R.J.: A diagnostic study of the diurnal rainfall variation in the gate b-scale area. Journal of the Atmospheric Sciences **38**(7), 1429–1445 (1981)
2. Albright, M.D., Recker, E.E., Reed, R.J., Dang, R.: The diurnal variation of deep convection and inferred precipitation in the central tropical pacific during januaryebruary 1979. Monthly Weather Review **113**(10), 1663–1680 (1985)
3. Betts, A.K.: Thermodynamic Classification of Tropical Convective Soundings. Monthly Weather Review **102**, 760–+ (1974)
4. Biello, J., Majda, A.: A multi-scale model for the madden–julian oscillation. J. Atmos. Sci. **62**, 1694–1721 (2005)
5. Chapin, F.S., Mooney, H., Chapin, H.C., Matson, P.: Principles of Terrestrial Ecosystem Ecology. Springer (2002)
6. Cohen, J.C.P., Silva Dias, M.A.F., Nobre, C.A.: Environmental conditions associated with amazonian squall lines: A case study. Monthly Weather Review **123**(11), 3163–3174 (1995)
7. Dai, A., Trenberth, K.E.: The diurnal cycle and its depiction in the community climate system model. Journal of Climate **17**(5), 930–951 (2004)
8. Emanuel, K.A.: An Air-Sea Interaction Model of Intraseasonal Oscillations in the Tropics. Journal of Atmospheric Sciences **44**, 2324–2340 (1987)
9. Frenkel, Y., Khouider, B., Majda, A.J.: Simple multicloud models for the diurnal cycle of tropical precipitation. part I: Formulation and the case of the tropical oceans. J. Atmos. Sci. p. Accepted (2010)
10. Frenkel, Y., Khouider, B., Majda, A.J.: Simple multicloud models for the diurnal cycle of tropical precipitation. part II: The continental regime. J. Atmos. Sci. p. Accepted (2010)
11. Frenkel, Y., Majda, A.J., Khouider, B.: Using the stochastic multicloud model to improve tropical convective parameterization: A paradigm example. J. Atmos. Sci. p. Accepted (2011)
12. Frierson, D.M.W., Kim, D., Kang, I.S., Lee, M.I., Lin, J.: Structure of AGCM-Simulated Convectively Coupled Kelvin Waves and Sensitivity to Convective Parameterization. Journal of Atmospheric Sciences **68**, 26–45 (2011)
13. Garreaud, R., Wallace, J.M.: The diurnal march of convective cloudiness over the americas. Monthly Weather Review **125**(12), 3157–3171 (1997)
14. Gill, A.E.: Atmosphere-Ocean Dynamics. Academic, San Diego, Calif. (1982)
15. Grabowski, W.W., Moncrieff, M.W.: Large-scale organization of tropical convection in two-dimensional explicit numerical simulations. Quarterly Journal of the Royal Meteorological Society **127**(572), 445–468 (2001)
16. Hendon, H.H., Woodberry, K.: The diurnal cycle of tropical convection. Journal of Geophysical Research **98**, 16,623–16,638 (1993)

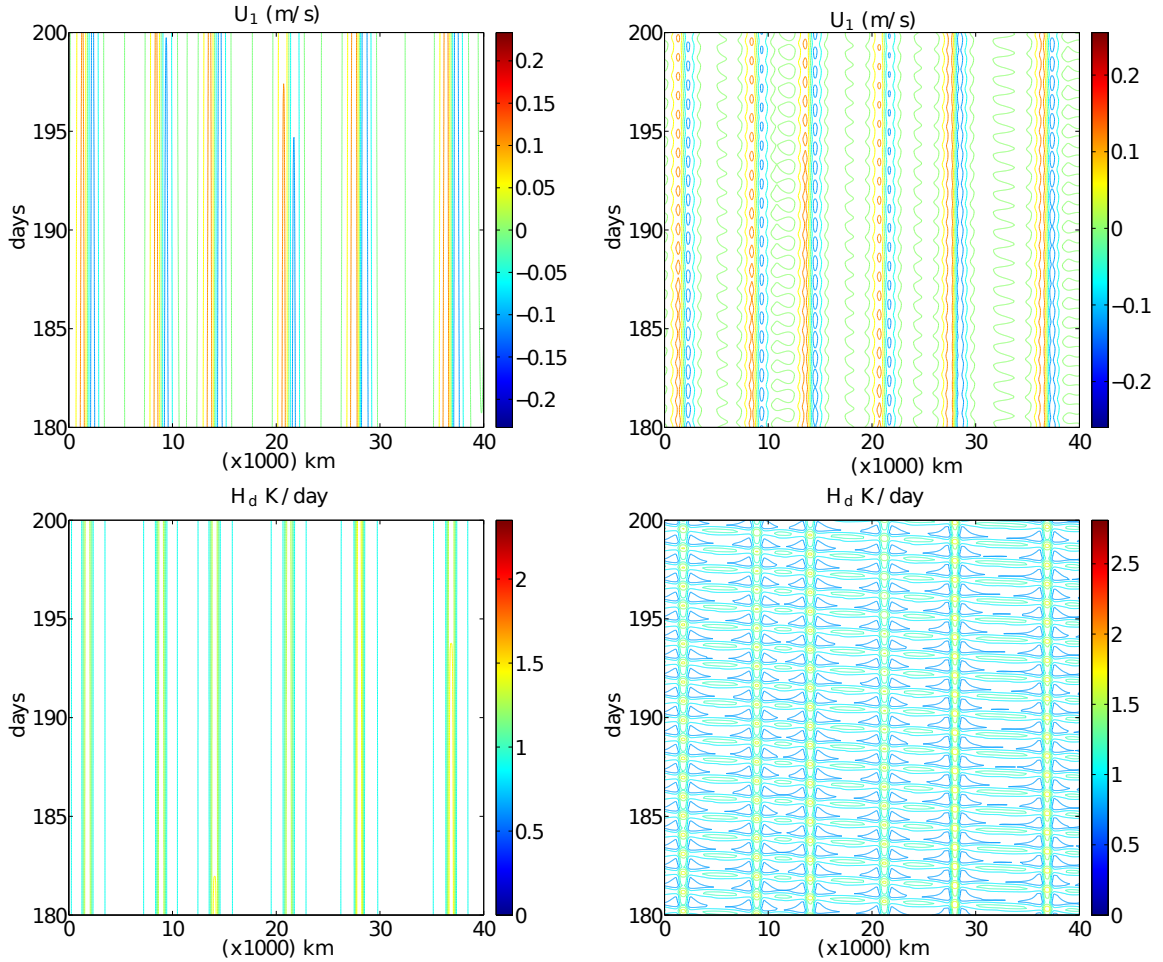

Fig. 12 Plot of $x-t$ contours of 1st baroclinic velocity and deep convective heating field over the last 20 days of simulation of reduced KM model, without (left) and with (right) diurnal cycle.

17. Houze Jr., R.A., Betts, A.K.: Convection in GATE. Reviews of Geophysics and Space Physics **19**, 541–576 (1981)
18. Hsu, S.A.: A relationship between the bowen ratio and sea — air temperature difference under unstable conditions at sea. J. Phys. Oceanogr. **28**, 2222–2226 (1998)
19. Itoh, H.: The Mechanism for the Scale Selection of Tropical Intraseasonal Oscillations. Part I: Selection of Wavenumber 1 and the Three-Scale Structure. Journal of Atmospheric Sciences **46**, 1779–1798 (1989)
20. Johnson, R.H., Rickenbach, T.M., Rutledge, S.A., Ciesielski, P.E., Schubert, W.H.: Trimodal characteristics of tropical convection. Journal of Climate **12**(8), 2397–2418 (1999)
21. Jordan, C.L.: Mean soundings for the west indies area. J. Meteor. **15**, 91–97 (1958)
22. Khouider, B., Biello, J., Majda, A.: A stochastic multicloud model for tropical convection. Commun. Math. Sci. **8**(1), 187–216 (2010)
23. Khouider, B., Han, Y., Biello, J.: Convective momentum transport in a simple multicloud model. J. Atmos. Sci. p. accepted (2011)
24. Khouider, B., Majda, A.J.: A non-oscillatory well balanced scheme for an idealized tropical climate model. Part I: Algorithm and validation. Theor. Comp. Fluid Dyn. **19**, 331–354 (2005)
25. Khouider, B., Majda, A.J.: A non-oscillatory well balanced scheme for an idealized tropical climate model. Part II: Nonlinear coupling and moisture effects. Theor. Comp. Fluid Dyn. **19**, 355–375 (2005)
26. Khouider, B., Majda, A.J.: Multicloud convective parametrizations with crude vertical structure. Theor. Comp. Fluid Dyn. **20**, 351?375 (2006)
27. Khouider, B., Majda, A.J.: A simple multicloud parametrization for convectively coupled tropical waves. part I: Linear analysis. J. Atmos. Sci. **63**, 1308–1323 (2006)
28. Khouider, B., Majda, A.J.: Equatorial convectively coupled waves in a simple multicloud model. J. Atmos. Sci. **65**, 3376–3397 (2008)

29. Khouider, B., Majda, A.J.: Multicloud models for organized tropical convection: Enhanced congestus heating. J. Atmos. Sci. **65**, 897–914 (2008)
30. Khouider, B., St-Cyr, A., Majda, A.J., Tribbia, J.: MJO and convectively coupled waves in a coarse resolution GCM with a simple multicloud parametrization. J. Atmos. Sci. p. *Submitted* (2010)
31. Kikuchi, K., Wang, B.: Diurnal precipitation regimes in the global tropics. J. Climate **21**, 2680–2696 (2008)
32. Kousky, V.E.: Diurnal rainfall variation in northeast brazil. Monthly Weather Review **108**(4), 488–498 (1980)
33. Krauss, E.B.: The diurnal precipitation change over the sea. J. Atmos. Sci. **20**, 551–556 (1963)
34. Liu, C., Moncrieff, M.W.: A numerical study of the diurnal cycle of tropical oceanic convection. J. Atmos. Sci. **55**(13), 2329–2344 (1998)
35. Majda, A., Biello, J.: A multi-scale model for the intraseasonal oscillation. Proc. Nat. Acad. Sci. **101**, 4736–4741 (2004)
36. Majda, A.J., Shefter, M.G.: Models for stratiform instability and convectively coupled waves. Journal of the Atmospheric Sciences **58**(12), 1567–1584 (2001)
37. Majda, A.J., Shefter, M.G.: Waves and instabilities for model tropical convective parameterizations. Journal of the Atmospheric Sciences **58**(8), 896–914 (2001)
38. Majda, A.J., Stechmann, S.N.: Stochastic models for convective momentum transport. Proceedings of the National Academy of Sciences **105**(46), 17,614–17,619 (2008)
39. Majda, A.J., Stechmann, S.N.: A simple dynamical model with features of convective momentum transport. Journal of the Atmospheric Sciences **66**(2), 373–392 (2009)
40. Mapes, B.E.: Convective Inhibition, Subgrid-Scale Triggering Energy, and Stratiform Instability in a Toy Tropical Wave Model. Journal of Atmospheric Sciences **57**, 1515–1535 (2000)
41. McGarry, M.M., Reed, R.J.: Diurnal Variations in Convective Activity and Precipitation During Phases II and III of GATE. Monthly Weather Review **106**, 101–+ (1978)
42. Moncrieff, M.W.: Organized convective systems: Archetypical dynamical models, mass and momentum flux theory, and parameterization. Quart. J. Roy. Meteor. Soc. **118**, 819–850 (1992)
43. Moncrieff, M.W., Liu, C.: Representing Convective Organization in Prediction Models by a Hybrid Strategy. Journal of Atmospheric Sciences **63**, 3404–3420 (2006). DOI 10.1175/JAS3812.1
44. Neelin, J.D., Yu, J.Y.: Modes of Tropical Variability under Convective Adjustment and the Madden-Julian Oscillation. Part I: Analytical Theory. Journal of Atmospheric Sciences **51**, 1876–1894 (1994)
45. Nesbitt, S.W., Zipser, E.J.: The diurnal cycle of rainfall and convective intensity according to three years of trmm measurements. Journal of Climate **16**(10), 1456–1475 (2003)
46. Randall, D.A., Harshvardhan, Dazlich, D.A.: Diurnal variability of the hydrological cycle in a general circulation model. Journal of the Atmospheric Sciences **48**(1), 40–62 (1991)
47. Ray, C.L.: Diurnal variation of rainfall at san juan, p. r.1. Monthly Weather Review **56**(4), 140–141 (1928)
48. Reed, R.J., Jaffe, K.D.: Diurnal variation of summer convection over west africa and the tropical eastern atlantic during 1974 and 1978. Monthly Weather Review **109**(12), 2527–2534 (1981)
49. Sably, M.L., Hendon, H.H., Woodberry, K., Tanaka, K.: Analysis of global cloud imagery from multiple satelittes. Bull. Amer. Meteor. Soc. **72**, 467–480 (1991)
50. Sadhuram, Y., Ramana Murthy, T.V., Sarma, Y.V.B., Murty, V.S.N.: Comments on ,on the estimation of overwater bowen ratio from sea air temperature difference. Journal of Physical Oceanography **31**(7), 1933–1934 (2001)
51. Slingo, J., Inness, P., Neale, R., Woolnough, S., Yang, G.: Scale interactions on diurnal toseasonal timescales and their relevanceto model systematic errors. Annals of Geophysics **46**(1) (2003)
52. Straub, K.H., Kiladis, G.N.: Observations of a convectively coupled kelvin wave in the eastern pacific itcz. J. Atmos. Sci. **59**, 30–53 (2002)
53. Sui, C.H., Li, X., Lau, K.M.: Radiative convective processes in simulated diurnal variations of tropical oceanic convection. Journal of the Atmospheric Sciences **55**(13), 2345–2357 (1998)
54. Takayabu, Y.N.: Large-scale cloud disturbances associated with equatorial waves. part I: Spectral features of the cloud disturbances. J. Meteor. Soc. Japan **72**(5), 433–448 (1994)
55. Tian, B., Soden, B.J., Wu, X.: Diurnal cycle of convection, clouds, and water vapor in the tropical upper troposphere: Satellites versus versus a general circulation model. J. Geophys. Res. Lett. **109**, D10,101, doi:10.1029/2001GL014,113. (2004)
56. Tian, B., Waliser, D.E., Fetzer, E.J., Lambrigtsen, B.H., Yung, Y.L., Wang, B.: Vertical moist thermodynamic structure and spatialtemporal evolution of the mjo in airs observations. J. Atmos. Sci. **63**(10), 2462–2485 (2006)
57. Tokioka, T., Yamazaki, K., A., K., Ose, T.: The equatorial 3060-day oscillation and the ArakawaSchubert penetrative cumulus parameterization. J. Meteor. Soc. Japan **66**, 883–901 (1988)
58. Waite, M.L., Khouider, B.: Boundary layer dynamics in a simple model for convectively coupled gravity waves. J. Atmos. Sci. **66**, 2780–2795 (2009)
59. Wallace, J.M.: Diurnal variations in precipitation and thunderstorm frequency over the conterminous united states. Monthly Weather Review **103**(5), 406–419 (1975)
60. Wang, W., Schlesinger, M.E.: The Dependence on Convection Parameterization of the Tropical Intraseasonal Oscillation Simulated by the UIUC 11-Layer Atmospheric GCM. Journal of Climate **12**, 1423–1457 (1999)
61. Wheeler, M., Kiladis, G.N.: Convectively coupled equatorial waves: Analysis of clouds and temperature in the wavenumber-frequency domain. J. Atmos. Sci. **56**(3), 374–399 (1999)
62. Wheeler, M., Kiladis, G.N., Webster, P.J.: Large-scale dynamical fields associated with convectively coupled equatorial waves. Journal of the Atmospheric Sciences **57**(5), 613–640 (2000)
63. Yang, G., Slingo, J.: The diurnal cycle in the tropics. Monthly Weather Review **129**(4), 784–801 (2001)

64. Yang, S., Smith, E.A.: Mechanisms for diurnal variability of global tropical rainfall observed from trmm. Journal of Climate **19**(20), 5190–5226 (2006)
65. Yano, J.I., Emanuel, K.: An Improved Model of the Equatorial Troposphere and Its Coupling with the Stratosphere. Journal of Atmospheric Sciences **48**, 377–389 (1991)
66. Yano, J.I., Moncrieff, M.W., McWilliams, J.C.: Linear stability and single-column analyses of several cumulus parametrization categories in a shallow-water model. Quarterly Journal of the Royal Meteorological Society **124**, 983–1005 (1998)
67. Zhang, G.J., Mu, M.: Simulation of the Madden Julian Oscillation in the NCAR CCM3 Using a Revised Zhang McFarlane Convection Parameterization Scheme. Journal of Climate **18**, 4046–4064 (2005)